USGS
science for a changing world

Shear Wave Velocity and Site Amplification Factors for 25 Strong-Motion Instrument Stations Affected by the *M*5.8 Mineral, Virginia, Earthquake of August 23, 2011

By Robert E. Kayen, Brad A. Carkin, Skye C. Corbett, Aliza Zangwill, Ivan Estevez, and Lena Lai

Open-File Report 2015–1099

U.S. Department of the Interior
U.S. Geological Survey

U.S. Department of the Interior
SALLY JEWELL, Secretary

U.S. Geological Survey
Suzette M. Kimball, Acting Director

U.S. Geological Survey, Reston, Virginia 2015

Suggested citation:
Kayen, R.E, Carkin, B.A., Corbett, S.C., Zangwill, Aliza, Estevez, Ivan, and Lai, Lena, 2015, Shear wave velocity and site amplification factors for 25 strong-motion instrument stations affected by the *M*5.8 Mineral, Virginia, earthquake of August 23, 2011: U.S. Geological Survey Open-File Report 2015–1099, 66 p., http://dx.doi.org/10.3133/ofr20151099.

ISSN 2331-1258 (online)

Contents

Figures

Tables

Shear Wave Velocity and Site Amplification Factors for 25 Strong-Motion Instrument Stations Affected by the *M*5.8 Mineral, Virginia, Earthquake of August 23, 2011

By Robert E. Kayen, Brad A. Carkin, Skye C. Corbett, Aliza Zangwill, Ivan Estevez, and Lena Lai

Abstract

Vertical one-dimensional shear wave velocity (V_s) profiles are presented for 25 strong-motion instrument sites along the Mid-Atlantic eastern seaboard, Piedmont region, and Appalachian region, which surround the epicenter of the *M*5.8 Mineral, Virginia, Earthquake of August 23, 2011. Testing was performed at sites in Pennsylvania, Maryland, West Virginia, Virginia, the District of Columbia, North Carolina, and Tennessee. The purpose of the study is to determine the detailed site velocity profile, the average velocity in the upper 30 meters of the profile ($V_{S,30}$), the average velocity for the entire profile ($V_{S,Z}$), and the National Earthquake Hazards Reduction Program (NEHRP) site classification. The V_s profiles are estimated using a non-invasive continuous-sine-wave method for gathering the dispersion characteristics of surface waves. A large trailer-mounted active source was used to shake the ground during the testing and produce the surface waves. Shear wave velocity profiles were inverted from the averaged dispersion curves using three independent methods for comparison, and the root-mean square combined coefficient of variation (COV) of the dispersion and inversion calculations are estimated for each site.

Introduction

This project focuses on the measurement of the shear wave velocity (V_s) of near-surface materials at strong-motion recording stations in the Mid-Atlantic states at sites where instruments recorded motions from the *M*5.8 Mineral, Virginia, earthquake. During two seasons of testing in 2011 and 2012, data were collected in Pennsylvania, Maryland, West Virginia, Virginia, the District of Columbia, North Carolina, and Tennessee. These states are regionally instrumented with permanent seismometer recording stations administered by a suite of entities: the U.S. Geological Survey (USGS) National Strong-Motion Project (NSMP), the USGS Advanced National Seismic System (ANSS), the Geological Survey of Pennsylvania (GSPA), USGS-NetQuakes, Lamont-Doherty Geologic Observatory, Virginia Tech University, Washington Monument National Mall (NAMA) and White House Ellipse National Park Service NetQuakes affiliate, and the Mineral Virginia site response temporary deployment.

The V_s profiles presented in this report are useful for calibration of site amplification models based on direct measurement of velocity, topography, or surface geologic unit. Data presented here were gathered using the continuous sine wave source spectral analysis of surface waves (CSS-SASW) test presented by Kayen and others (2004), which uses a stepped-sine method similar to that of the University of Texas and a wave-notch-filtered technique of receiving signals that improves on the approach of Satoh and others (1991). The unique aspect of the USGS surface wave vibration system is a large parallel array of electromechanical shakers mounted to a trailer frame that is transported to each

site. The trailer is called the Velociraptor. The CSS-SASW technique is an inexpensive and efficient means of non-invasively estimating the near-surface V_s of the ground. Though it is possible to measure V_s in cased boreholes or during penetration tests, these approaches tend to be not useful for evaluation of any of the strong-motion sites tested in this study as they cannot reach the meaningful depths required for seismic site response analysis without expensive drilling and casing. Because many of the sites are located in or near the Appalachian Mountains with thin soil cover over in-place weathered rock, penetration methods are not useful.

The V_s profiles presented in this report—for local site conditions in six states and the District of Columbia, tested between December 8, 2011, and June 27, 2012—are reported in tables 1 and 2.

Table 1. Shear wave velocity testing sites in Mid-Atlantic states in 2011 and 2012, site data.
[Columns (left to right) record (1) the U.S. Geological Survey (USGS) station name; (2) seismometer station location; (3) latitude (LAT); (4) longitude (LONG); (5) seismometer station owner/operator; (6) date of data collection]

USGS site	Location	LAT	LONG	Operator	Date tested
935RES	Reston Fire Station, Reston, Va.	38.9505	-77.33614	NSMP, 2555	December 8, 2011
936CBN	USGS CORBIN Observatory, Fredericksburg, Va.	38.20361	-77.37281	ANSS Backbone, USCBN	December 8, 2011
938MAR	Martinsburg VA Hospital, Martinsburg, W. Va.	39.41641	-77.90707	NSMP, 2511	April 24, 2012
939PAG	Penn. Geological Survey, Harrisburg, Pa.	40.2271	-76.7232	GSPA.PAGS	April 25, 2012
940MVL	Millersville Univ., Millersville, Pa.	39.9992	-76.3506	Lamont-Doherty. MVL	April 25, 2012
941PSB	Penn. State Univ., Brandywine, Pa.	39.92696	-75.4512	GSPA, PSUB	April 26, 2012
942DXL	Drexel University, Lancaster Ave, Philadelphia, Pa.	39.9571	-75.1896	NSMP, 2648	April 27, 2012
943WNC	Washington National Cathedral, Washington, D.C.	38.9301	-77.0706	NetQuakes, WNC WNC—NQ—01	April 28, 2012
944MIN	Mineral, Va.	38.02831	-77.84045	NSMP, 2560	April 28, 2012
945JSR	J. Sargeant Reynolds C.C., Goochland, Va.	37.6952	-77.8798	Virginia Tech, JSRW	April 28, 2012
946CMB	Cumberland Volunteer Fire Station, Cumberland, Va.	37.4881	-78.563	NSMP, 2558	April 29, 2012
947UVR	University of Richmond, Richmond, Va.	37.5709	-77.534	Virginia Tech, URVA	April 29, 2012
948LWR	Mineral area near Lake Anne, Va.	38.07712	-77.75008	NetQuakes, GS.LWRD	April 30, 2012
949NQ1	USGS National Headquarters, Reston, Va.	38.936	-77.332	NetQuakes, RestonUSGS NQ1	April 30, 2012

USGS site	Location	LAT	LONG	Operator	Date tested
950PRB	Giles County Courthouse, Pearlsburg, Va.	37.3275	-80.7345	NSMP, 2549	June 11, 2012
951ETU	James H. Quillen College of Medicine & VA Medical Center, Eastern Tennessee State Univ., Johnson City, Tenn.	36.307	-82.37951	NSMP, 2405	June 13, 2012
952ASH	Charles George VA Hospital, Asheville, N.C.	35.5912	-82.4844	NSMP. 2510	June 13, 2012
953TZN	Tazewell, Tenn.	36.5433	-83.5504	USGS. USTZTN	June 13, 2012
954SAL	W. G. (Bill) Hefner VA Medical Center, Salisbury, N.C.	35.6851	-80.4888	NSMP, 2506	June 14, 2012
955WM	Washington Monument, Sylvan Stage, East Ellipse, Washington, D.C.	38.6885	-77.0346	Washington Monument $NAMA_r$	June 15, 2012
956PRZ	White House, Presidents Park, Ellipse, Washington, D.C.	38.8952	-77.0394	NetQuakes, CAPTL	June 15, 2012
957SI	Smithsonian Institution, Museum Support Facilities, Suitland, Md.	38.84198	-76.94073	Mineral, Virginia Site Response	June 26, 2012
958NNC	Cliffs of the Neuse State Park, Seven Springs, N.C.	35.2398	-77.8906	ANSS Backbone, USCNNC	June 26, 2012
959MWV	West Virginia Geological & Economic Survey, Morgantown, W. Va.	39.658	-79.846	ANSS Backbone, USMCWV	June 27, 2012

Table 2. Shear wave velocity testing sites in Mid-Atlantic states in 2011 and 2012, measured site parameters.
[Columns (left to right) record (1) the U.S. Geological Survey (USGS) site name; (2–3) depth of investigation by forward and manual inversions, in meters (m); (4–5) maximum shear wave velocity of forward and manual inversion profiles, in meters per second (m/s); (6–7) site parameter V_{S30}, defined as 30 meters divided by the shear wave travel time to 30 meters depth, for forward and manual inversions, in meters per second (m/s); (8–9) average shear wave velocity of entire profile, for forward and manual inversions, in meters per second (m/s); and (10) National Earthquake Hazards Reduction Program (NEHRP) site classifications]

USGS site	Depth of investigation (m)		$V_{s,max}$ (m/s)		$V_{s,30}$ (m/s)		Average V_s for entire profile (m/s)		Site class (NEHRP)
	Forward	Manual	Forward	Manual	Forward	Manual	Forward	Manual	
935RES	38	42	821	634	341	364	382	413	D
936CBN	64	65	364	389	269	280	312	320	D
938MAR	42	49	828	1,133	372	389	437	482	C
939PAG	36	43	325	242	431	525	353	362	C
940MVL	69	47	2,735	2,107	720	672	1,182	873	C

941PSB	46	50	1,336	1,243	353	391	452	515	C
942DXL	59	50	1,856	1,588	617	609	871	781	C
943WNC	44	50	690	664	353	357	403	426	C
944MIN	71	81	1,099	959	526	607	713	738	C
945JSR	34	35	786	916	481	477	502	515	C
946CMB	65	65	865	959	371	362	500	488	C
947UVR	50	50	749	758	351	359	429	450	D
948LWR	66	66	964	1,096	329	325	499	498	D
949NQ1	49	51	2,100	2,043	648	655	856	882	C
950PRB	30	30	883	824	523	498	523	498	C
951ETU	30	30	1,810	1,171	711	633	711	633	C
952ASH	42	49	721	788	359	358	418	444	D
953TZN	31	31	1,168	1,376	709	714	718	727	C
954SAL	30	31	1,492	1,340	396	431	396	437	C
955WM	64	70	1,011	1,095	346	342	484	502	D
956PRZ	64	69	1,021	1,052	342	334	480	487	D
957SI	80	82	609	628	275	272	393	397	D
958NNC	65	68	425	417	296	286	335	332	D
959MWV	38	40	2,992	2,379	1,465	1,483	1,632	1,645	B

The Mid-Atlantic sites tested in 2011 and 2012 are plotted on regional maps in figures 1 through 4. The National Earthquake Hazards Reduction Program (NEHRP) A–E site classification is as follows: (1) blue square, A; (2) green circle, B; (3) yellow diamond, C; (4) red triangle, D; and (5) purple triangle, E. Figures 5 through 8 show the Velociraptor SASW trailer positioned at several sites during typical testing conditions.

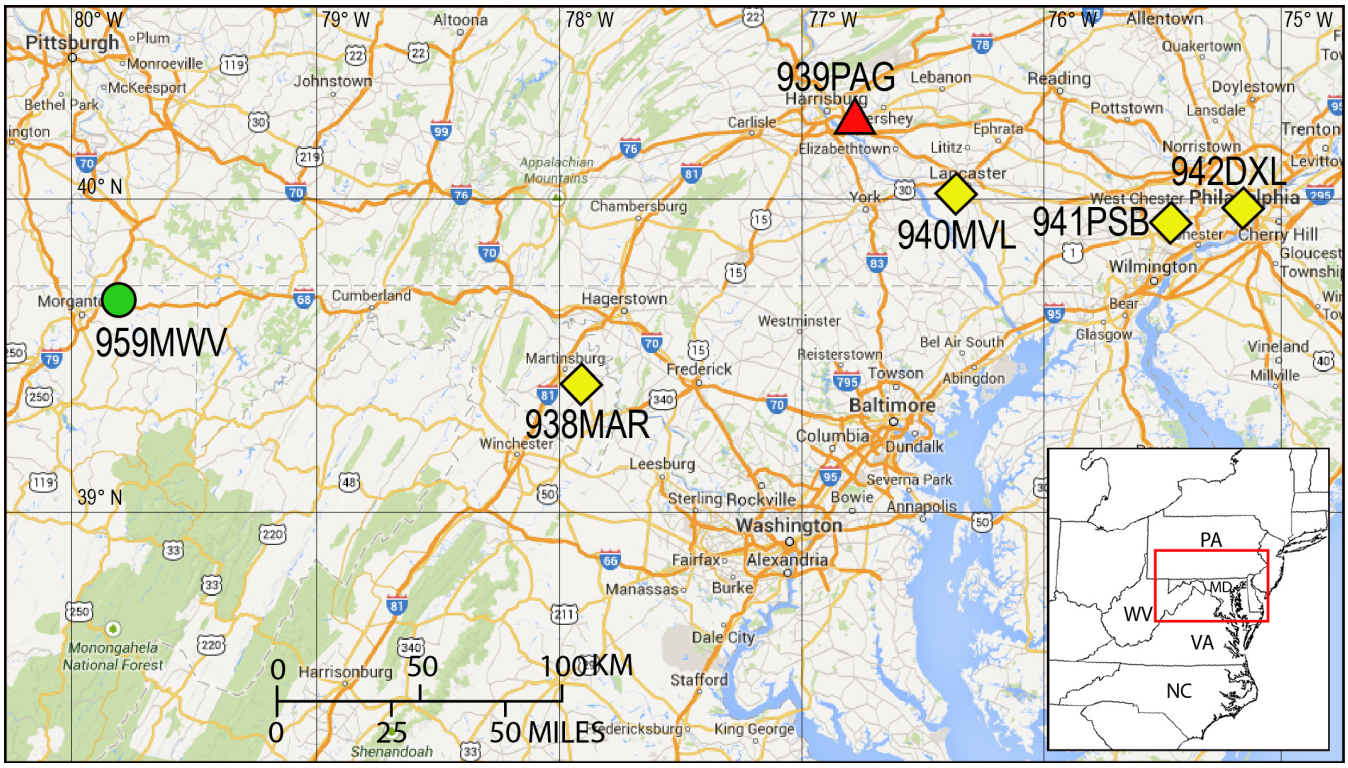

Figure 1. Map showing spectral analysis of surface waves (SASW) test sites visited in Pennsylvania, West Virginia, and Virginia in 2012. Symbols indicate National Earthquake Hazards Reduction Program site classifications, where green circle is a B site, yellow diamonds are C sites, and red triangle is a D site.

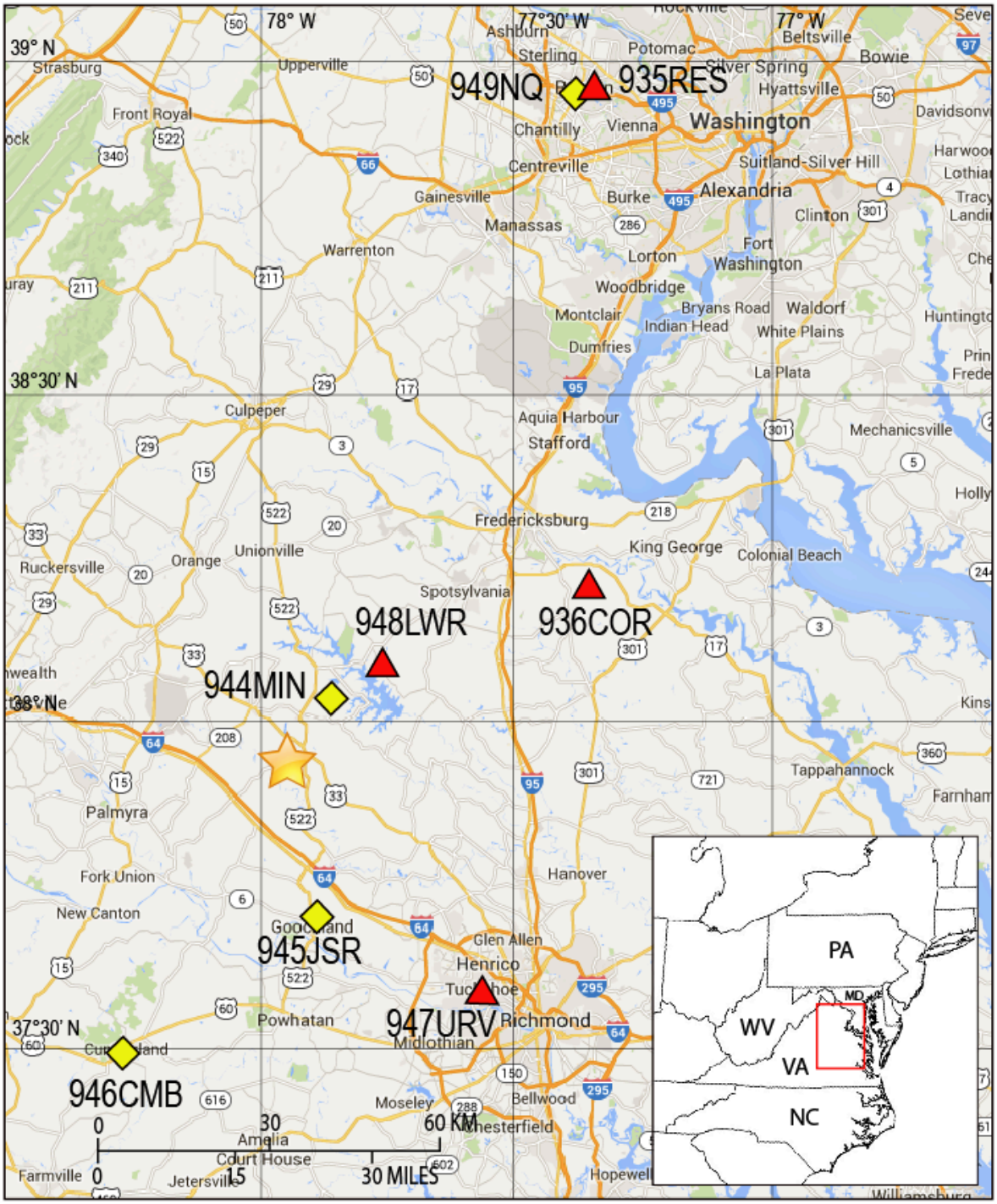

Figure 2. Map showing spectral analysis of surface waves (SASW) test sites visited in Virginia in 2011 and 2012. Symbols indicate National Earthquake Hazards Reduction Program site classifications, where yellow diamonds are C sites and red triangles are D sites. The epicenter of the *M*5.8 Mineral, Virginia, earthquake of August 23, 2011, is shown by the yellow star.

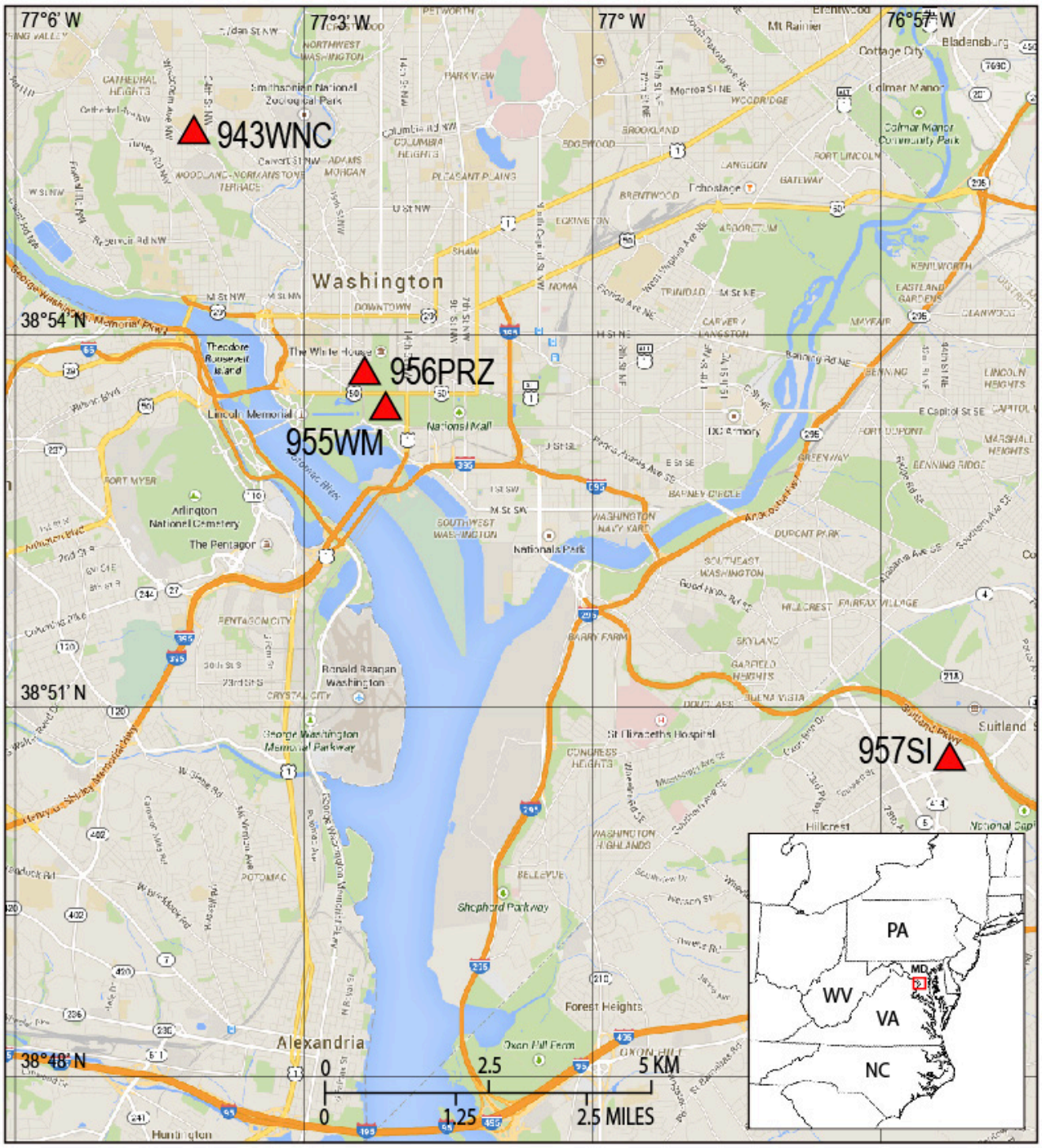

Figure 3. Map showing spectral analysis of surface waves (SASW) test sites visited in Washington, D.C., and vicinity in 2012. Symbols indicate National Earthquake Hazards Reduction Program site classifications, where red triangles are D sites.

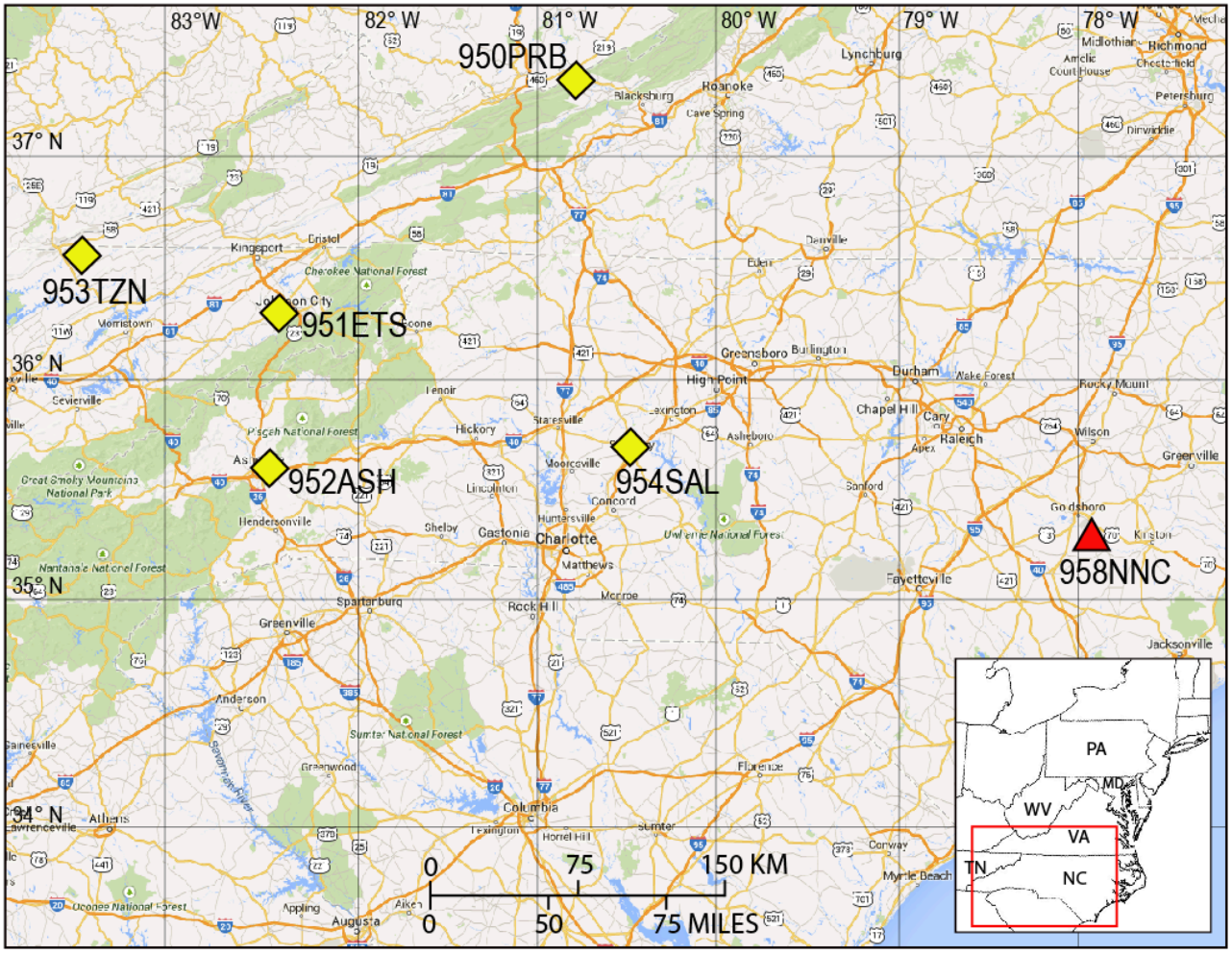

Figure 4. Map showing spectral analysis of surface waves test sites (SASW) visited in Virginia, North Carolina, and Tennessee in 2012. Symbols indicate National Earthquake Hazards Reduction Program site classifications, where yellow diamonds are C sites and red triangle is a D site.

Figure 5. The U.S. Geological Survey Velociraptor spectral analysis of surface waves (SASW) trailer ready for testing, positioned southeast of the Washington Monument in front of the Sylvan Theater stage, site 955WM, on June 15, 2012.

Figure 6. The U.S. Geological Survey Velociraptor spectral analysis of surface waves (SASW) trailer positioned at the south transept of the Washington National Cathedral, site 943WNC, on April 28, 2012.

Figure 7. The USGS Velociraptor spectral analysis of surface waves (SASW) trailer set up for testing at site 935RES on December 8, 2012. The red, 11-kilowatt generator at the back of the trailer powers all equipment during testing.

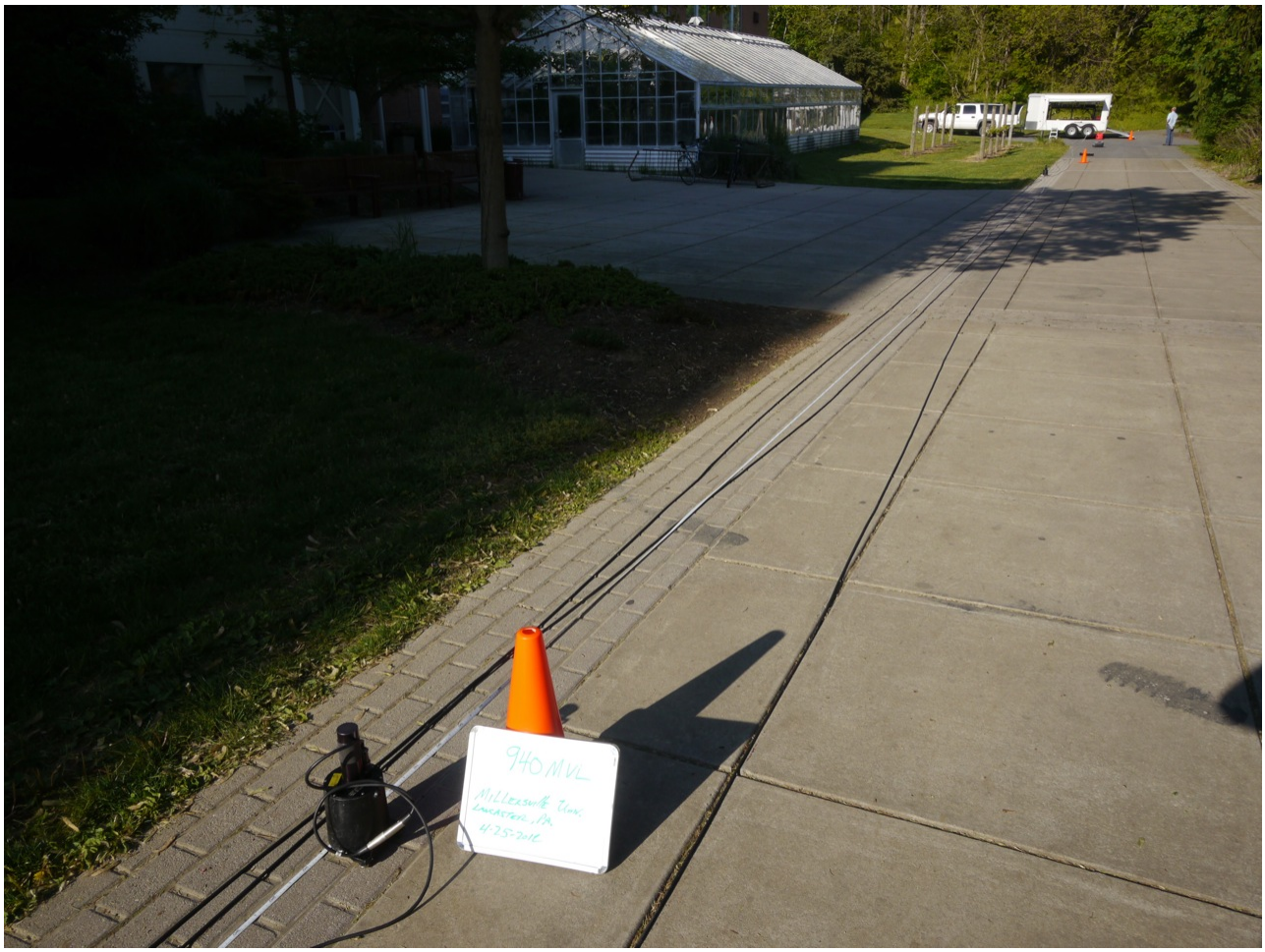

Figure 8. Seismometer array set up adjacent to Caputo Hall, Millersville University, Millersville, Pennsylvania, site 940MVL, on April 25, 2012. The USGS Velociraptor spectral analysis of surface waves (SASW) trailer is at the far end of the array.

Rayleigh Wave Dispersion

Active-source surface wave analysis testing typically profiles the upper tens of meters of the ground using drop weights or harmonic sources. The upper 30 meters (m) are needed to compute the widely used site parameter $V_{S,30}$, defined as 30 m divided by the shear wave travel time to a depth of 30 m. The SASW method employed in this study by the USGS is a technique that uses a parallel array of mass shakers. This method allows for profiling to 100 m without the use of massive drop weights or heavy track-mounted machinery. For this method, we substitute an array of many low frequency (1–100 hertz [Hz]) electromechanical shakers. Surface waves are generated with an array of between two and eight APS Dynamics Model 400 shakers and amplifier units, powered by a generator and controlled by a spectral analyzer.

The shakers have a long stroke capable of cycling to as low as 1 Hz. The output signal from the spectral analyzer is split into a parallel circuit and sent to the separate amplifiers. The amplifiers power the shakers to produce a continuously vibrating, coherent, in-phase harmonic wave that vertically loads the ground. Most of this energy produces Rayleigh retrograde elliptical surface waves that propagate away from the source in a vertical, cylindrical wavefront perpendicular to the ground surface. The

amplitude of the surface waves decay exponentially with depth, such that the energy of the wavefront is centered at a depth of approximately one-third to one-half the wavelength.

Frequency-domain analyses are made on two or more signals received by sensors placed in the field in the linear array some distance from the source. First, all channels of time-domain data are transformed into their equivalent linear spectrum in the frequency domain using a Fourier transform. One of the sensor's signals (typically the sensor closest to the source) is used for a reference input signal, and the other sensor signals are used to compute the linear spectra of the output. The separation distance from the reference seismometer to each output seismometer ($d_s - d_{ref}$) is later used to compute the wave velocity. The cross power spectrum $G_{xy}(\omega)$ is determined by multiplying the complex conjugate of the linear spectrum of the input signal $S_x^*(\omega)$ and the real portion of the linear spectrum of the output signal $S_y(\omega)$. The cross power spectrum is defined as

$$G_{xy}(\omega) = S_x^*(\omega) \times S_y(\omega) \tag{1}$$

The autopower spectrum, a measure of the energy at each frequency of the sweep, can be used to determine the strength of individual frequencies and is equal to the linear spectrum of a given sensor times its complex conjugate pair:

$$G_{xx}(\omega) = S_x(\omega) \times S_x^*(\omega), \text{ and} \tag{2}$$

$$G_{yy}(\omega) = S_y(\omega) \times S_y^*(\omega). \tag{3}$$

A cross power spectrum can be represented by its real and imaginary components for its phase, θ, and magnitude, m. The phase is the relative lag between the signals at each frequency, and the magnitude is a measure of the power between the two signals at each frequency. Because the phases are relative, they can be stacked to enhance signal-to-noise ratio of the phase lag at each frequency.

The phase of the cross power spectrum is computed as the inverse tangent of the ratio of the imaginary and real portions of the cross power spectrum:

$$\theta_{xy}(\omega) = \tan^{-1}\frac{Im(G_{xy}(\omega))}{Re(G_{xy}(\omega))} \tag{4}$$

The travel time $t(f)$ of one cycle of a wave of frequency (f) is computed as

$$t(f) = \theta(\omega)/\omega \tag{5}$$

and the wavelength, λ, at each frequency is

$$\lambda(\theta) = (d_s - d_{ref})/\theta(f) \tag{6}$$

The Rayleigh wave velocity, V_r , is computed as

$$\begin{aligned} V_r(f) &= (d_s - d_{ref})/t(f) \\ &= f(d_s - d_{ref})\ 360°/\theta \text{ (degrees)} \\ &= f(d_s - d_{ref})\ 2\pi/\theta(\phi) \text{ (radians)} \\ &= f\lambda(f) \end{aligned} \tag{7}$$

The SASW procedure maps the change in θ across the frequency spectrum and merges these phase lags with the sensor array geometry to measure velocity. Typically, with the shaker source, the discrete frequencies are cycled in a swept-sine (stepped) fashion across a range of low frequencies (1–200 Hz). Rayleigh wave phase velocity is then mapped in frequency or wavelength space. This velocity map or profile is called a dispersion curve and characterizes changes in the frequency-dependent

Rayleigh wave velocity. The evaluation of velocities is constrained to the wavelength zone where $\lambda(f)/3 < (d_s - d_{ref}) < 2\lambda(f)$ for typical data and $\lambda(f)/3 < (d_s - d_{ref}) < 3\ \lambda(f)$ for excellent data, corresponding to phase lags of 180°–1,080° (typical data) and 120°–1,080° (excellent data). At longer and shorter wavelengths, the data become unreliable for computing velocities.

Because the usable wavelengths are constrained by the seismometer separation, the array is expanded to capture Rayleigh wave dispersion representative of a specific range of wavelengths. The near surface is characterized by short wavelengths and high frequencies, whereas the deeper portion of the profile is characterized by long wavelengths and low frequencies. Each wavelength range requires a separate independent test that is merged together with other wavelength ranges to determine an average dispersion curve for the site.

At the largest seismometer separations, the increasing area of the wavefront causes the wave amplitude to diminish, owing to geometric damping, and the overall quality of the data diminishes. Two measures of data quality are used to evaluate the field measurements in the frequency domain. Coherence, $\gamma^2(\omega)$, is a normalized real function with values between 0 and 1, corresponding to the ratio of the power of the cross power spectrum, $G_{yx}(\omega) \bullet G_{yx}^{*}(\omega)$, to the autopower spectrum of the outboard seismometer, $G_{xx}(\omega) \bullet G_{yy}(\omega)$. Values close to 1 indicate high correlation between the reference and outboard seismometers across narrow frequency bands. This is a useful data quality parameter for hammer impact data.

$$\gamma_{xy}^2(\omega) = \frac{G_{yx}(\omega) \bullet G_{yx}^{*}(\omega)}{G_{xx}(\omega) \bullet G_{yy}(\omega)} \tag{8}$$

For swept-sine data, where discrete frequencies are used to compute phase rather than narrow frequency bands, the frequency response function (FRF) is a complex measure of the data quality of the output (outboard) seismometer and is sometimes called the transfer function:

$$\mathrm{FRF}(\omega) = \frac{G_{yx}(\omega)}{G_{xx}(\omega)} \tag{9}$$

where x is the input (reference) signal and y is the response (output) signal.

The frequency response function is a two-sided complex parameter. To convert to the frequency response gain (magnitude) that is used to evaluate the amplitude of the output response to the input stimulus, a rectangular-to-polar coordinate conversion is used.

Adjustments for Missing 1st Wrapped Phase

At some sensor separations, the field data have a poorly formed 1st phase such that the first clear wrapped-phase crossing occurs not at 180°, but at 540°. For these dispersion data files, a simple reprocessing was done to add one phase jump (360°, 2π) to the dispersion curves preceding the 540° jump to adjust the file to the correct wrapped-phase number. This adjustment corrects the wavelength calculation as follows:

$$\lambda_{(corrected)} = 2\pi d/(\theta + 2\pi) \tag{10}$$

With the wavelength adjusted, the velocity, V_r, decreases by

$$V_r = f \bullet 2\pi d/(\theta + 2\pi) \tag{11}$$

The effect of correcting the phase wrap and reducing the calculated wavelength is to reduce the depth of influence of the adjusted dispersion curve.

Inversion of the V_s Profile

The relation between Rayleigh wave (V_R), shear wave (V_S) and compression wave (V_P) velocities can be formulated through Navier's equations for dynamic equilibrium. On the surface of the ground, and in the case of plane strain, the following characteristic equation can be applied:

$$\frac{V_r}{V_s}^6 - 8\,\frac{V_r}{V_s}^4 + \left(24 - 16\left[\frac{1-2\nu}{2(1-\nu)}\right]\right)\frac{V_r}{V_s}^2 + 16\left[\left[\frac{1-2\nu}{2(1-\nu)}\right] - 1\right] = 0 \tag{12}$$

where ν is the Poisson ratio and

$$\frac{V_S}{V_P} = \gamma = \sqrt{\left[\frac{1-2\nu}{2(1-\nu)}\right]} \tag{13}$$

For reasonable values of Poisson ratio for earth materials, between 0.30 and 0.49, Viktorov (1967) shows that the shear wave velocity ranges between 105 and 115 percent of the measured Rayleigh wave velocity.

$$\frac{V_R}{V_S} = K = \frac{0.87+1.12\nu}{1+\nu} \tag{14}$$

such that across the range $0.2 < \nu < 0.49$, the range of K is $0.87 < K < 0.96$.

The inversion method seeks to infer an acceptable best-fit model of seismic shear wave velocity, V_S, of the ground given the measured dispersive characteristics of Rayleigh waves observed in the frequency domain and the estimated profile of Poisson ratio and material density. The inversion attempts to build a model from observations, as opposed to the normal prediction of behavior based upon a model. If the inversion model is simple and linear, it will result in a unique and stable solution. The French mathematician Hadamard defined mathematical problems that have solutions that exist, are unique, and are stable as "well-posed" (Zhdanov, 2002). On the other hand, surface wave inversion is an "ill-posed" inverse problem, as solutions are not unique, the solutions may become unstable, and multiple shear wave velocity profiles can result in approximately the same dispersion curve (Hisada, 1994; Zhdanov, 2002).

The dispersive characteristic of Rayleigh wave propagation allows us to infer the V_S at depth based on measurements at the free surface. The inversion problem computes the Rayleigh wave phase velocity (V_R) from laterally constant layers of an infinite half space. For each of these layers, the shear modulus, Poisson ratio, density, and thickness are unknown. Displacements for a vertically acting harmonic point load can be computed as follows in the far field if we neglect body wave components:

$$u_\beta(r,z,\omega) = F_z \cdot G_\beta \cdot (r,z,\omega) \cdot e^{i[\omega t - \psi_\beta(r,z,\omega)]} \tag{15}$$

where β stands for the generic component either vertical or radial, $G_\beta(r,z,\omega)$ is the Rayleigh geometrical spreading function, and $\Psi_\beta(r,z,\omega)$ is the composite phase function (Lai and Rix, 1998).

Regularization methods have been developed for solving the ill-posed inversion problem: for example, the velocity profiles computed here. The Levenberg-Marquardt method, also called damped least squares, is one example of a regularization method. These and other techniques, such as artificial neural networks and genetic algorithms, are discussed by Santamarina and Fratta (1998). One cost of these stochastic methods is that they often require many more iterations, and so they are much more computationally intensive.

The parameters of the inversion problem can be chosen such that the difference between the observational dispersion data and the output of the inversion problem are minimized. Such a constraint is insufficient for ill-posed problems because many solutions can fit the data equally well and some of these solutions will be physically unrealistic. The most common approach is to constrain the inversion solution space by selecting the smoothest solution from a suite of solutions that all exhibit a sufficient goodness-of-fit to the observed data, as indicated by a root-mean-square (RMS) error minimum (Constable and others, 1987).

An empirical approach serves as a counterpoint to the inversion methods used in this report. Pelekis and Athanasopoulos (2011) advanced the work of Satoh and others (1991) in a technique termed the SIM (simplified inversion method) that computes the shear wave velocity profile as a function of the incremental slope of the Rayleigh wave dispersion curve, where D_n is the depth at layer n:

$$V_{Sn,normal\ dispersion} = 1.1 \cdot \frac{\bar{V}_{Rn} D_n - \bar{V}_{Rn-1} D_{n-1}}{D_n - D_{n-1}} \tag{16}$$

$$V_{Sn,inverted\ dispersion} = 1.1 \cdot \frac{D_n - D_{n-1}}{D_n/\bar{V}_{Rn} - D_{n-1}/\bar{V}_{Rn-1}} \tag{17}$$

The dispersion curve, V_R, plotted against λ_R is converted into an apparent velocity ($\bar{V}_R$) and depth (z) by converting λ_R to an estimated depth of $z_{eq} = a_R \cdot \lambda_R \approx 0.635\lambda_R$. The parameter a_R is a penetration depth coefficient optimized to achieve a minimum weighted average difference between the simplified velocity profile and that computed through the more advanced inversion of Pelekis and Athanasopoulos (2011). The apparent phase velocity, $\overline{V_R}$, is approximated as the velocity at each segment node (layer interface) of a multilinear curve fit to the dispersion curve. A positive slope of a segment indicates normal dispersion; a negative slope indicates inverted dispersion. The value of V_s for each individual layer is calculated using the equations above for the cases of normal dispersion or inverted dispersion, respectively. The approach of Pelekis and Athanasopoulos (2011) improves on the Satoh and others (1991) method notably by optimizing the penetration depth coefficient a_R.

Results

We provide two profile solutions at each site (inversion and SIM). We varied the assumptions about the layer thicknesses and the threshold RMS error that determines if the inversion has converged to best characterize the site. The decision as to whether or not the more complex model is warranted by the fit of the theoretical dispersion curve (TDC) to the empirical dispersion curve (EDC) is subjective. Table 1 summarizes results and provides the SASW site ID, the site description, the date of data collection, the latitude and longitude of the SASW test site, and the V_{S30}.

Appendix A includes plots of the model profiles and the EDC and TDCs for each site. Appendix A also includes the site photos and a vicinity map for each site. Where possible, we have indicated the location of the strong-motion station in the site photographs and vicinity maps to assess the distance between the SASW survey and the strong-motion station. NEHRP classification is used to average the site conditions in the upper 30 m of ground ($V_{s,30}$ from the IBC, 2002). Equation 18 is used to compute this average velocity based on the unit layer thickness (d_i) and the corresponding interval-velocity (V_{Si}).

$$V_{Si-depth-averaged} = \frac{\sum_{i=1}^{n} d_i}{\sum_{i=1}^{n} \frac{d_i}{V_{Si}}} \tag{18}$$

These site categories are used to assign design spectra in the evaluation of performance for new and built structures.

A statistical analysis of the shear wave velocity of the upper 30 m was computed by determining the average coefficient of variation (COV_{DIS}) of the dispersion curve from the group phase velocity and the average coefficient of variation (COV_{INV}) of shear wave velocity profiles computed in the inversions that satisfied the minimum acceptable inversion model variance.

The mean values of the group dispersion curves where calculated by binning the dispersion curve values in terms of wavelength (for example, in 1-m bins) or frequency (for example, 1-Hz bins), and then averaging the values within each bin. The coefficient of variation was calculated by dividing the binned standard deviation of the velocity values by the binned mean values. The mean and standard deviation of the shear wave velocity layers of the inversion were calculated by averaging the layer values for the suite of profiles that satisfy the lowest possible root-mean-square error, separating the theoretical inversion-based and empirical field-dispersion curves.

For both the dispersion curve and the inversion-based coefficients of variation, the average coefficient of variation was determined for the profiles. The overall model coefficient of variation was computed as the root-mean-square of the dispersion COV and the inversion COV (equation 19).

$$COV_{MODEL} = \sqrt{COV_{DIS}{}^2 + COV_{INV}{}^2} \tag{19}$$

For the deep, stiff soil sites, the combined dispersion and inversion COV was typically less than 0.07, reflecting the remarkably good dispersion data sets and the gentle monotonic increasing nature of the velocity profiles. For sites situated on rock, the combined COV ranges from 0.12 to 0.23, reflecting greater variance in the field-dispersion data and the inverted profiles.

Site Data

The following pages present the individual site location photographs, location map, field and computed velocity data, dispersion curves, and inversion profiles. *Vs* values for 30 meters and the maximum profile depth are presented for the three inversion methods as well as the coefficient of variation of these parameters.

Resources

We have used the SWAMI Fortran routines that are freely available at http://geosystems.ce.gatech.edu/soil_dynamics/research/surfacewavesanalysis/ (distributed under the terms of the GNU General Public License).

Acknowledgments

This work is supported through the USGS Earthquake Science Center and the USGS Pacific Science Center.

References Cited

Constable, S.C., Parker, R.L., and Constable, G.G., 1987, Occam's inversion—A practical algorithm for generating smooth models from electromagnetic sounding data: Geophysics, v. 52, no. 3, p. 289–300.

Hisada, Y., 1994, An efficient method for computing Green's functions for a layered half-space with sources and receivers at close depths: Bulletin of the Seismological Society of America, v. 84, no. 5, p. 1456–1472.

Kayen, R., Seed, R.B., Moss, R.E. Cetin, O., Tanaka, Y., and Tokimatsu, K., 2004, Global shear wave velocity database for probabilistic assessment of the initiation of seismic-soil liquefaction: Proceedings of the 11th International Conference on Soil Dynamics and Earthquake Engineering, Berkeley, Calif., 2004, v. 2, p. 506–512.

Lai, C.G., and Rix, G.J., 1998, Simultaneous inversion of Rayleigh phase velocity and attenuation for near-surface site characterization: Georgia Institute of Technology, School of Civil and Environmental Engineering, Report No. GIT-CEE/GEO-98-2, 258 p.

Pelekis, P.C., and Athanasopoulos, G.A., 2011, An overview of surface wave methods and a reliability study of a simplified inversion technique. Soil Dynamics and Earthquake Engineering, v. 32, no. 12, p. 1654–1668, doi:10.1016/j.soildyn.2011.06.012.

Santamarina, J.C., and Fratta, D., 1998, Introduction to discrete signals and inverse problems in civil engineering: Reston, Va., American Society of Civil Engineers Press, 327 p.

Satoh, T., Poran, C.I., Yamagata, K., and Rondriquez, J.A., 1991, Soil profiling by spectral analysis of surface waves, *in* Proceedings of the Second International Conference On Recent Advances in Geotechnical Earthquake Engineering and Soil Dynamics, Vol. II, St. Louis, Mo., March 11–15, 1991: University of Missouri-Rolla, Paper No. 10.23, p.1429–1434.

Zhdanov, M.S., 2002, Geophysical inverse theory and regularization problems; Methods in Geochemistry and Geophysics, 36: Amsterdam, Elsevier, 628 p.

Appendix 1. Site Summaries

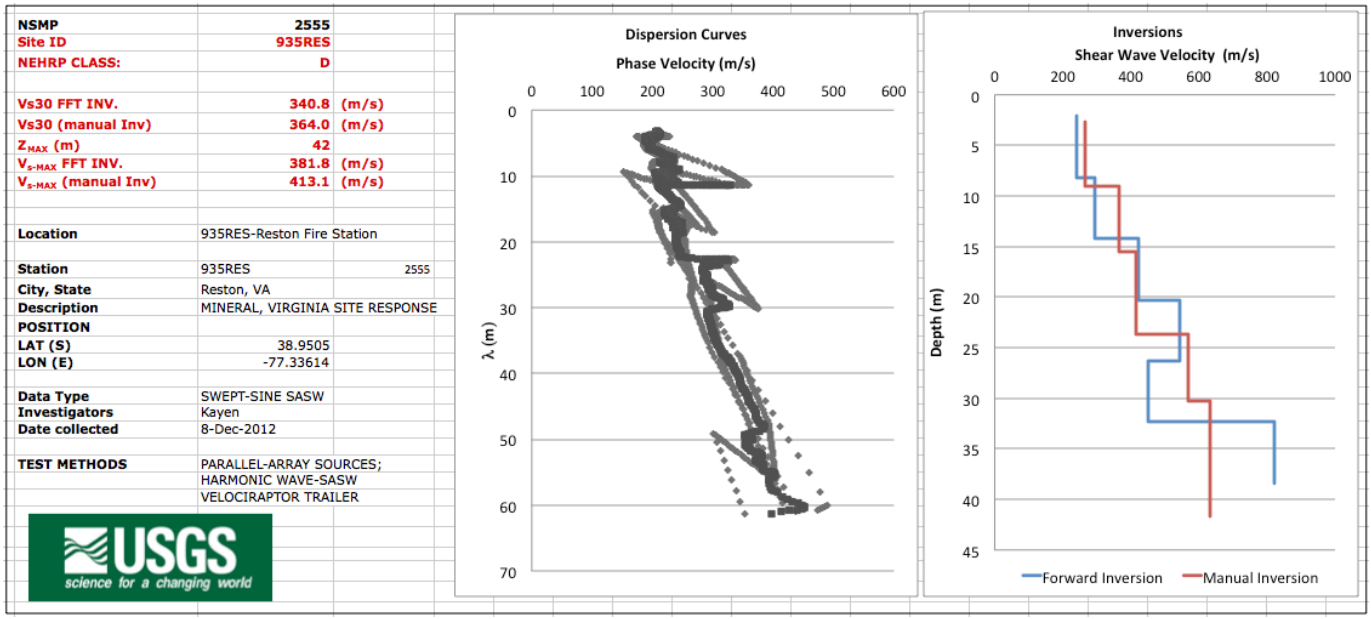

Figure 1–1. Site ID, location, and average shear wave velocity (left) for surface wave test site 935RES; average dispersion curve in black and individual empirical dispersion curves in gray (center plot); shear wave velocity profile computed by two inversion methods (right plot).

Figure 1–2. Surface wave test site 935RES located on the Washington and Old Dominion Trail (W&OD) at the intersection of Wiehle Avenue and Sunset Hills Road, Reston, Virginia (lat 38.9505, long −77.3361). A, View looking west down the seismometer array on the W&OD. B, Closer view of the shaker trailer. C, View looking east. D, USGS seismometer located in the fire station on Wiehle Avenue adjacent to the test site. E, Satellite view of the local site, yellow bar is seismometer array. F, Site location in Virginia near Washington, D.C.

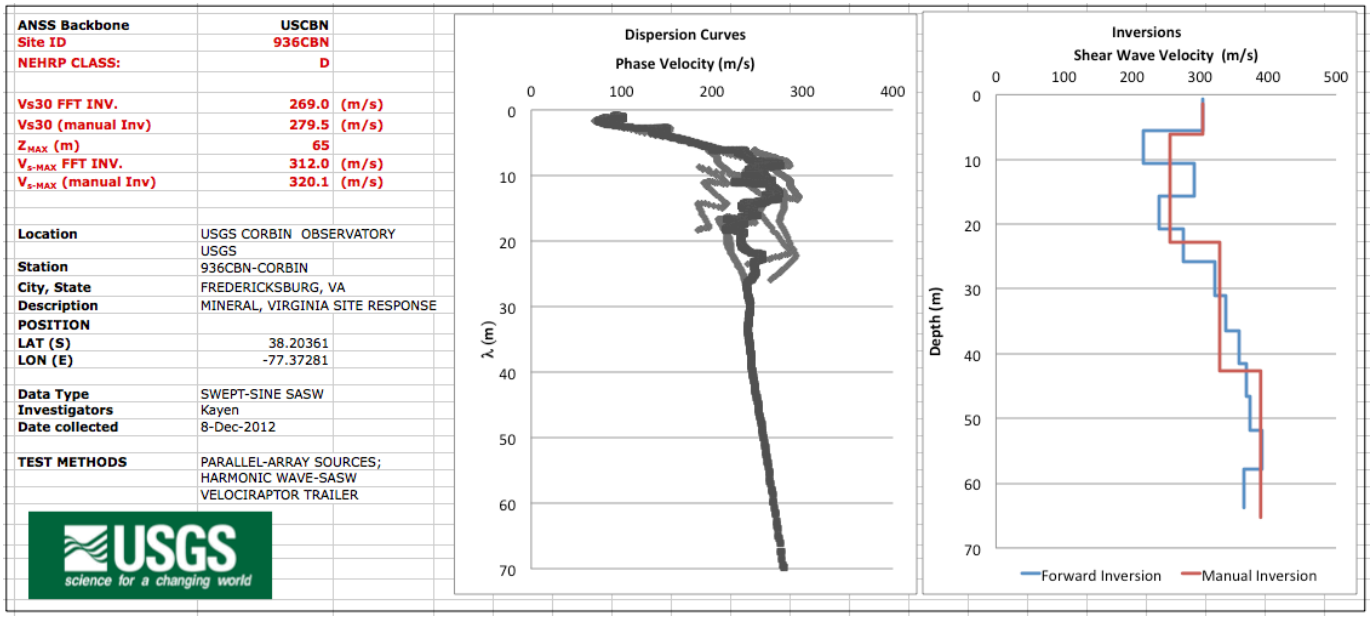

Figure 1–3. Site ID, location, and average shear wave velocity (left) for surface wave test site 936CBN; average dispersion curve in dark gray and individual empirical dispersion curves in lighter gray (center plot); shear wave velocity profiles computed by two inversion methods (right plot).

Figure 1–4. Surface wave test site 936CRB located at the Fredericksburg Geomagnetic Center, Corbin, Virginia (lat 38.2037, long −77.3728). A, View northward towards the seismometer array. B, Another view northward from the shaker trailer. C, View northwest at the shaker trailer. D, Sign at the entrance to the observatory. E, Satellite view of the local site, yellow bar is seismometer array. F, Site location in Virginia, 82 kilometers south-southwest of Washington, D.C.

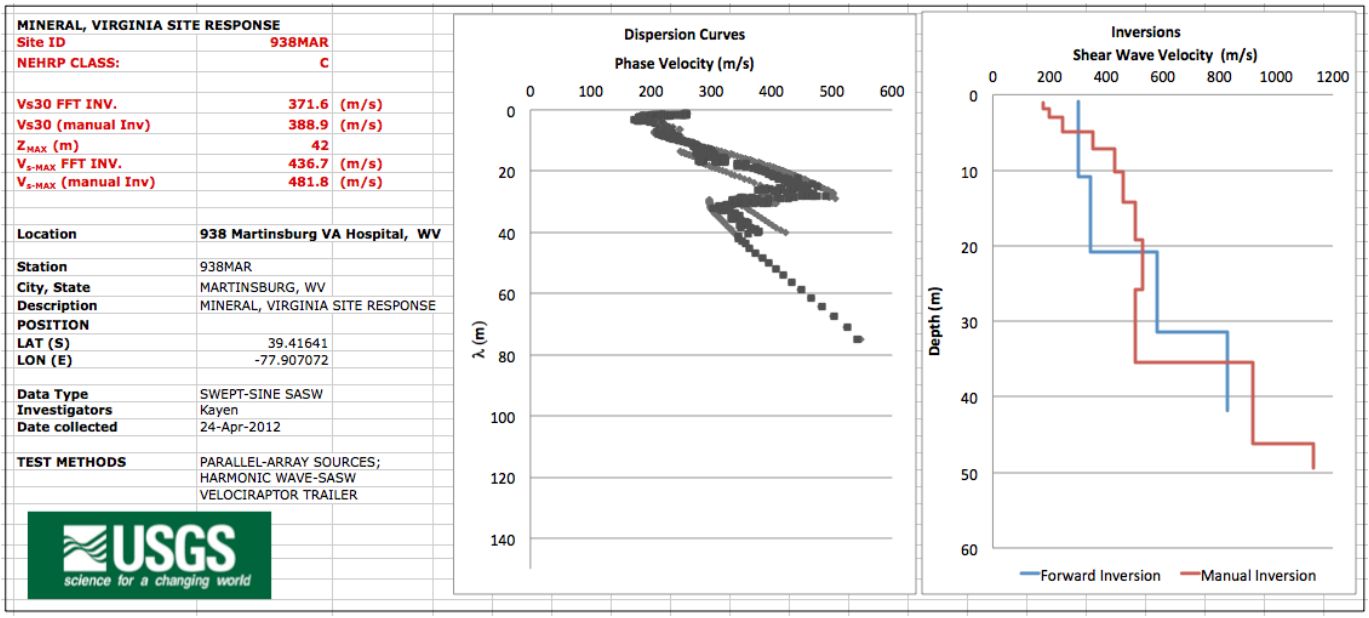

Figure 1–5. Site ID, location, and average shear wave velocity (left) for surface wave test site 938MAR; average dispersion curve in dark gray and individual empirical dispersion curves in lighter gray (center plot); shear wave velocity profiles computed by two inversion methods (right plot).

Figure 1–6. Surface wave test site 938MAR located at the Martinsburg VA Medical Center, Martinsburg, West Virginia (lat 39.4161, long −77.9068). A, View looking north along the seismometer array. B, View southward to the shaker trailer. C, View to the west from the shaker trailer. D, Another view to the west from the shaker trailer. E, Satellite view of the local site, yellow bar is seismometer array. F, Site location in Martinsburg, W. Va.

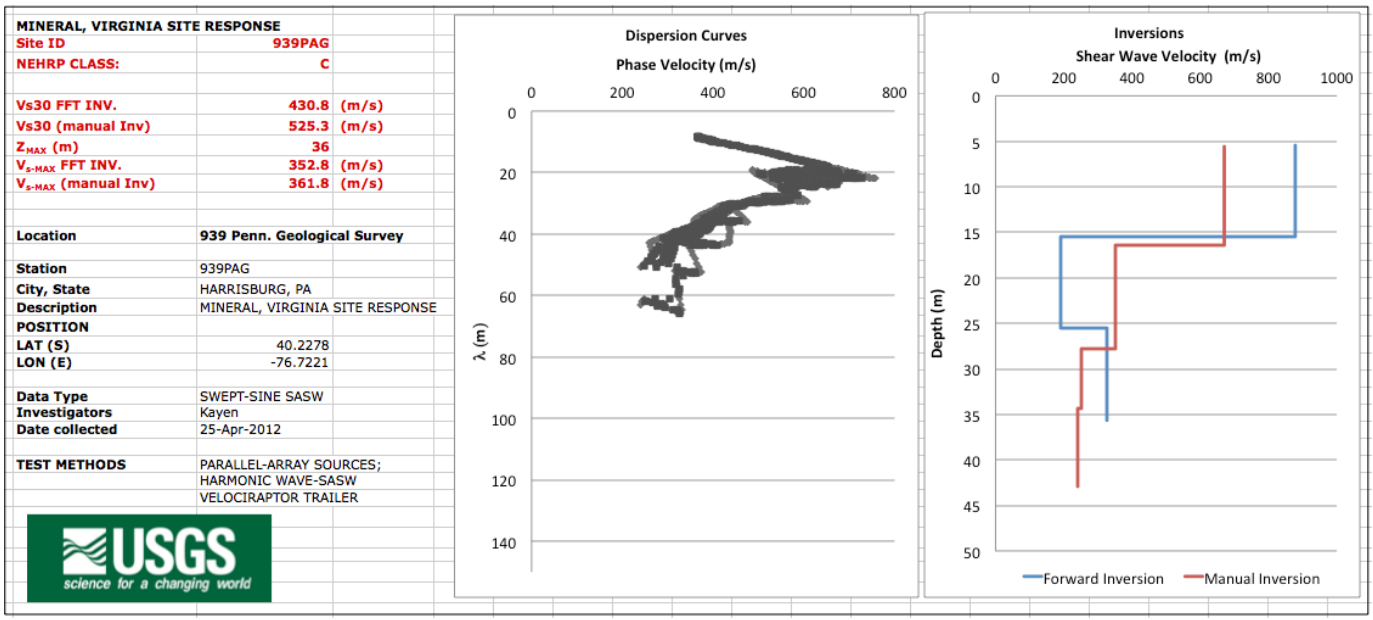

Figure 1–7. Site ID, location, and average shear wave velocity (left) for surface wave test site 939PAG; average dispersion curve in dark gray and individual empirical dispersion curves in lighter gray (center plot); shear wave velocity profiles computed by two inversion methods (right plot).

Figure 1–8. Surface wave test site 939PAG located at the Pennsylvania Geological Survey, Middletown, Pennsylvania (lat 40.2271, long −76.7232). A, View looking southwest in the direction of the seismometer array. B, View northwest to the shaker trailer. C, View northeast from the shaker trailer. D, Another view to the northeast at the shaker trailer location. E, Satellite view of the local site, yellow bar is seismometer array. F, Site location in Middletown, Pa.

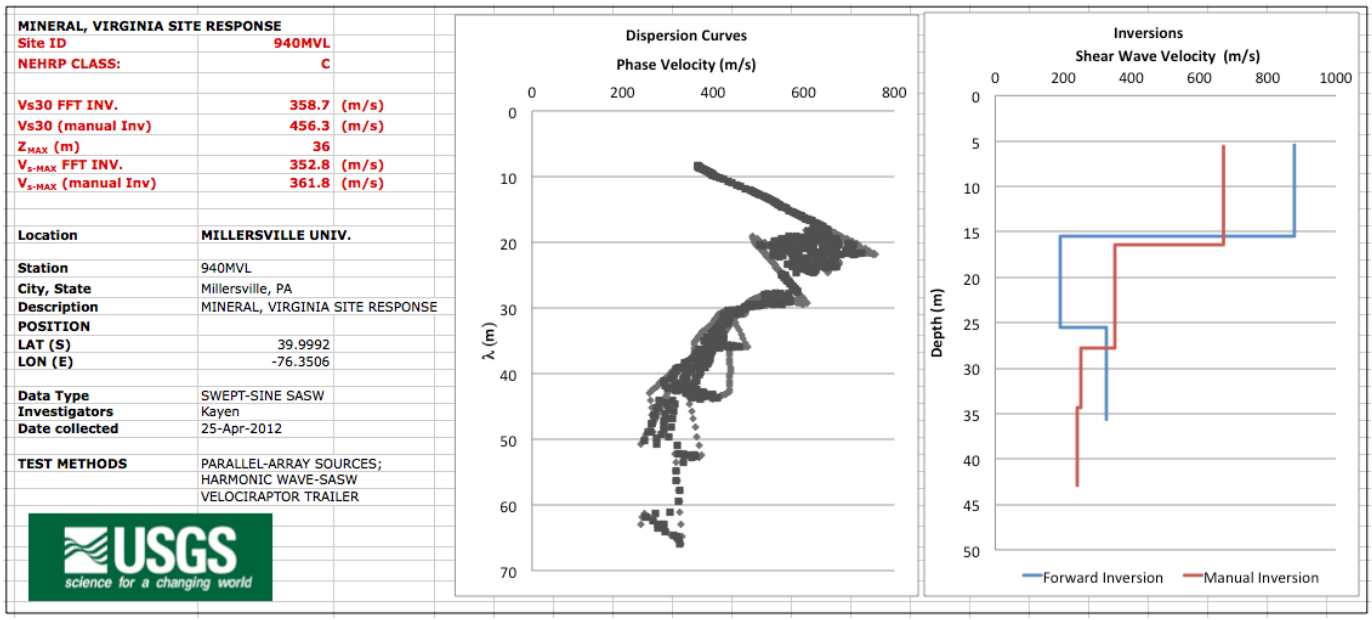

Figure 1–9. Site ID, location, and average shear wave velocity (left) for surface wave test site 940MVL; average dispersion curve in dark gray and individual empirical dispersion curves in lighter gray (center plot); shear wave velocity profiles computed by two inversion methods (right plot).

Figure 1–10. Surface wave test site 940MVL located adjacent to Caputo Hall, Millersville University, Millersville, Pennsylvania (lat 39.9992, long −76.3490). A, View looking westward along the seismometer array on an extension of E. Frederick Street. B, View eastward to the shaker trailer. C, Another view eastward to the shaker trailer. D, View eastward from near the end of the seismometer array. E, Satellite view of the local site, yellow bar is seismometer array. F, Site location in Millersville, Pa.

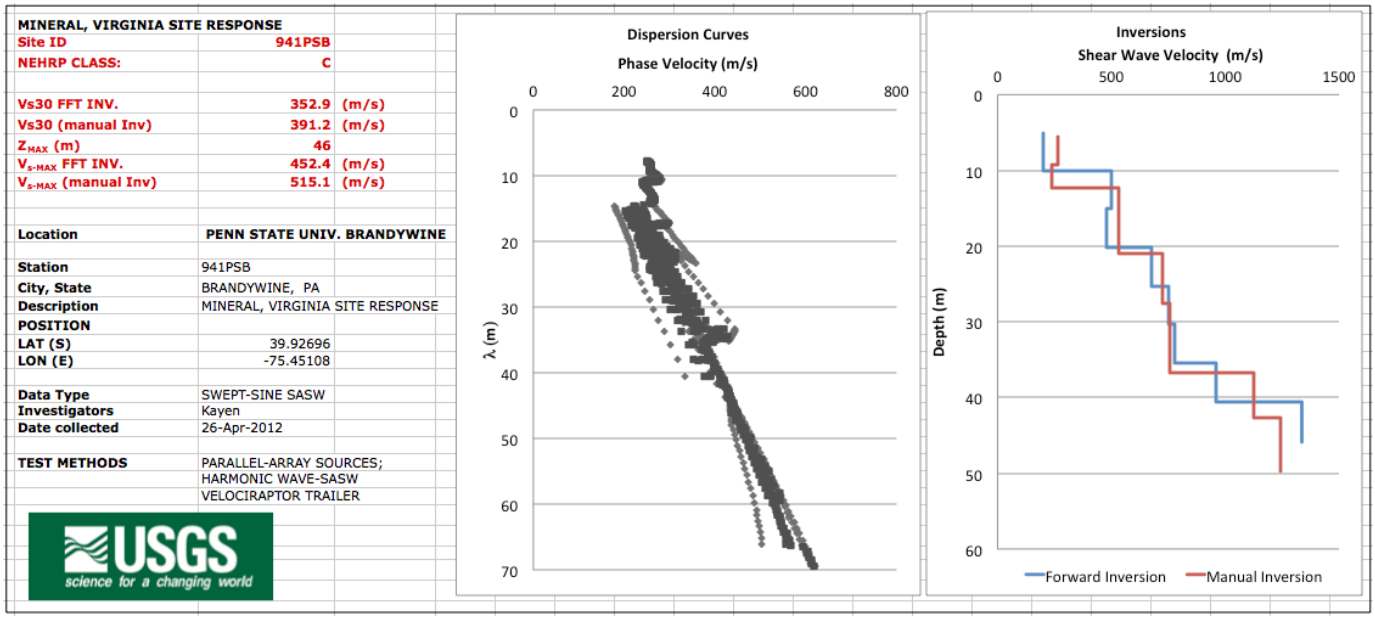

Figure 1–11. Site ID, location, and average shear wave velocity (left) for surface wave test site 941PSB; average dispersion curve in dark gray and individual empirical dispersion curves in lighter gray (center plot); shear wave velocity profiles computed by two inversion methods (right plot).

Figure 1–12. Surface wave test site 941PSB located at the maintenance building on the Pennsylvania State University Brandywine campus in Media, Pennsylvania (lat 39.9270, long −75.4512). A, View looking southeast towards the shaker trailer. B, View southwest along the seismometer array from the shaker trailer. C, View northeast toward the shaker trailer. D, Looking north to the shaker trailer with the maintenance building in the background. E, Satellite view of the local site, yellow bar is seismometer array. F, Site location in Media, Pa.

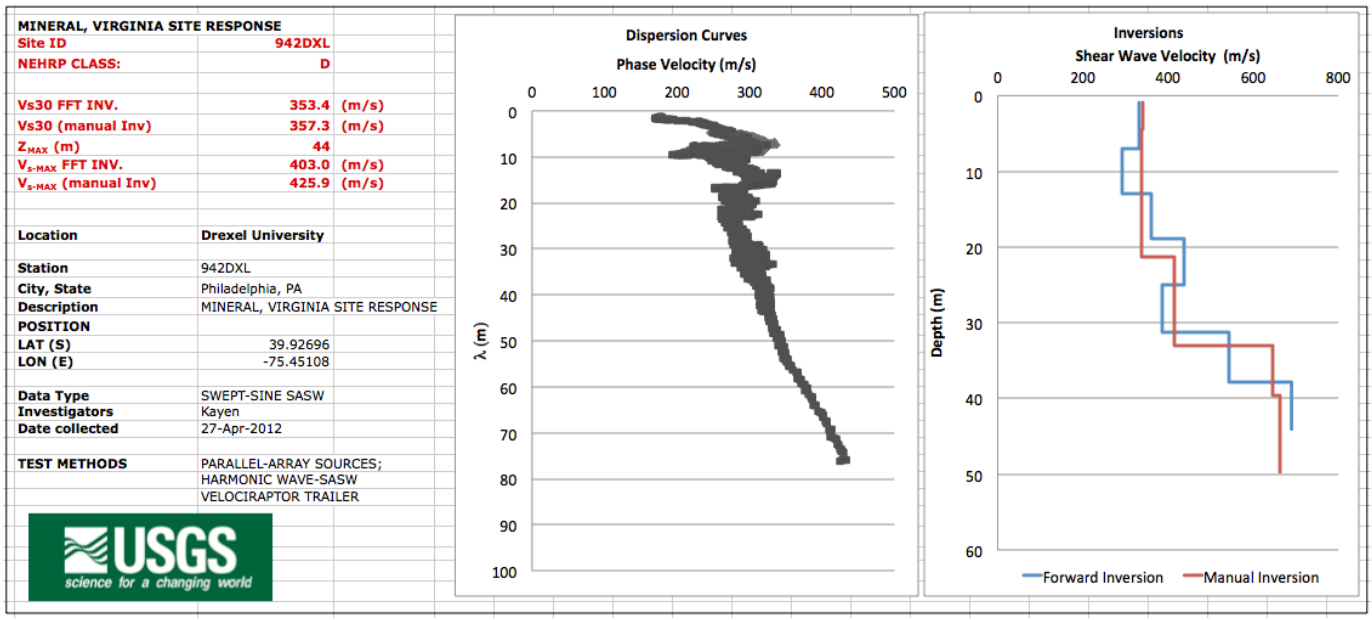

Figure 1–13. Site ID, location, and average shear wave velocity (left) for surface wave test site 942DXL; average dispersion curve in dark gray and individual empirical dispersion curves in lighter gray (center plot); shear wave velocity profiles computed by two inversion methods (right plot).

Figure 1–14. Surface wave test site 942DXL located on Cuthbert Street on the Drexel University campus, Philadelphia, Pennsylvania (lat 39.9571, long −75.1896). A, View looking southeast towards the shaker trailer. B, View northwest to the shaker trailer, Rush Building on the left. C, View westward down the seismometer array. D, View eastward along the seismometer array. E, Satellite view of the local site, yellow bar is seismometer array. F, Site location in Philadelphia, Pa.

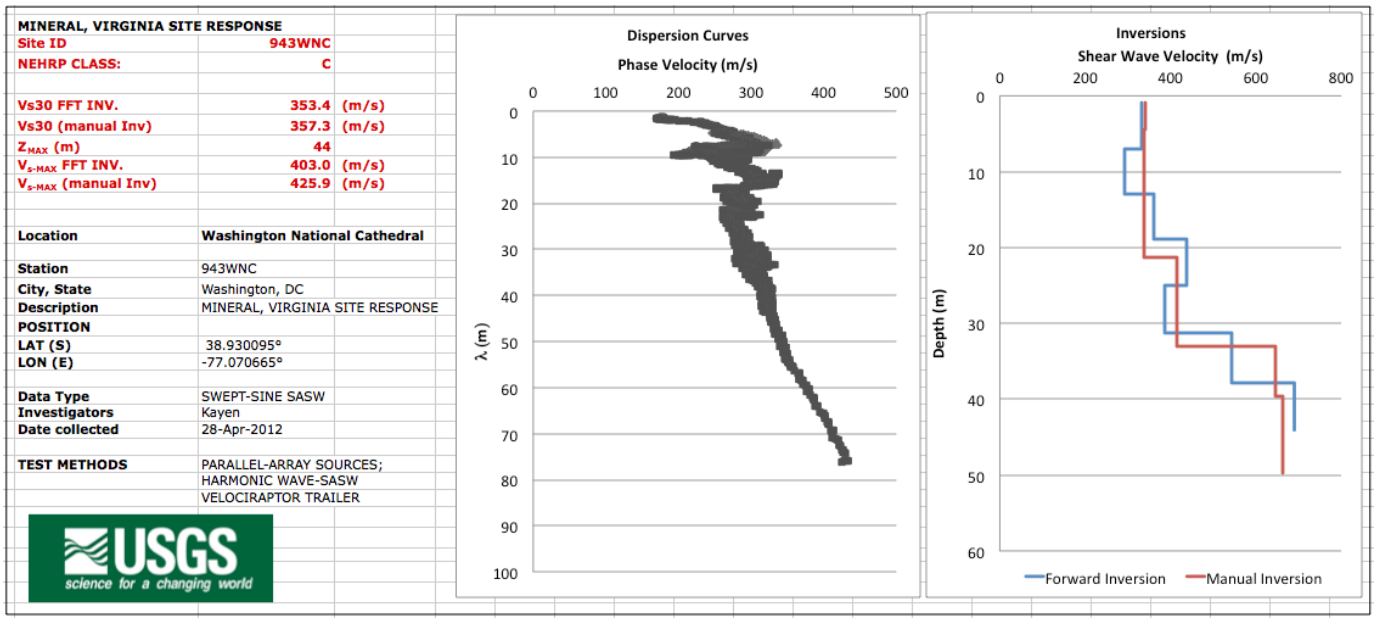

Figure 1–15. Site ID, location, and average shear wave velocity (left) for surface wave test site 943WNC; average dispersion curve in dark gray and individual empirical dispersion curves in lighter gray (center plot); shear wave velocity profiles computed by two inversion methods (right plot).

Figure 1–16. Surface wave test site 943WNC located at the Washington National Cathedral, Washington, D.C. (lat 38.9301, long −77.0706). A, View looking northwest towards the shaker trailer at the south transept of the cathedral. B, View westward to the seismometer array. C, View east along the seismometer array toward the shaker trailer. D, View to the northeast toward the shaker trailer. E, Satellite view of the local site, yellow bar is seismometer array. F, Site location in Washington, D.C.

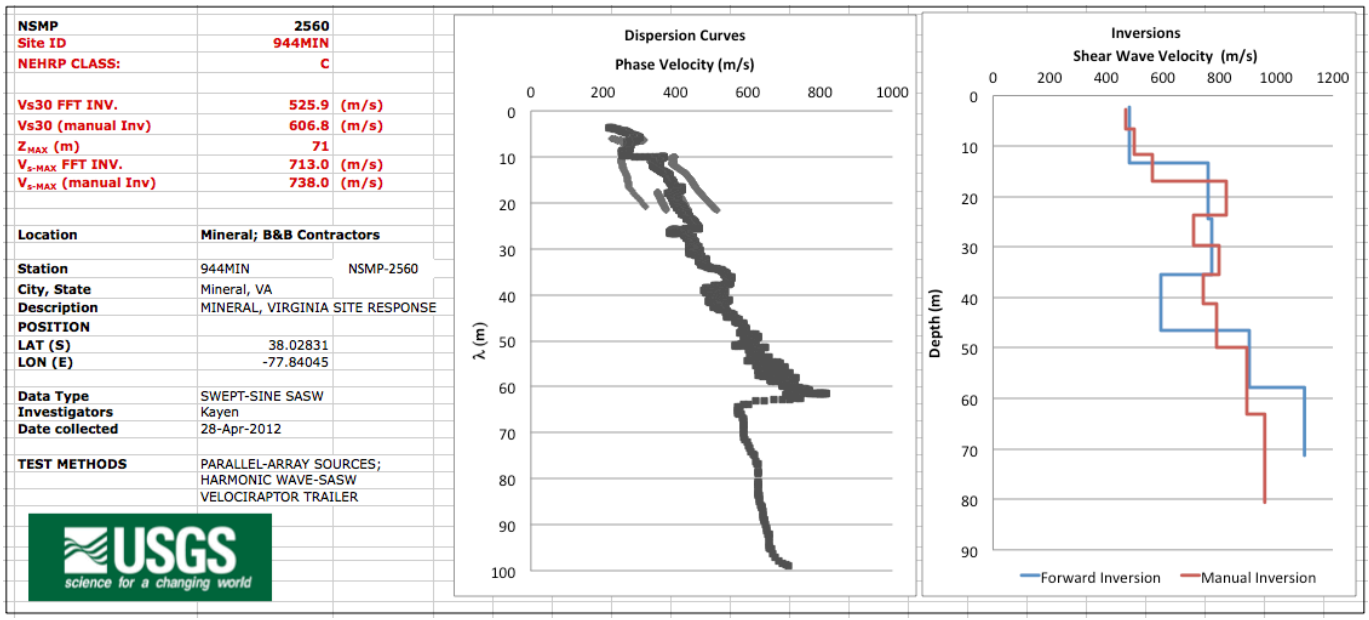

Figure 1–17. Site ID, location, and average shear wave velocity (left) for surface wave test site 944MIN; average dispersion curve in dark gray and individual empirical dispersion curves in lighter gray (center plot); shear wave velocity profiles computed by two inversion methods (right plot).

Figure 1–18. Surface wave test site 944MIN located 6.5 km NE of Mineral, Virginia (lat 38.0289, long −77.8421). Testing took place on a dirt road between State Route 700 and railroad tracks. A, Photo looking northeast from the shaker trailer down the seismometer array, railroad tracks on the left. B, View looking southwest toward the shaker trailer. C, Another view southwest to the shaker trailer. D, The shaker trailer parked at the Mineral fire station. E, Satellite view of the local site, yellow bar is seismometer array. F, Site location near Mineral, Va.

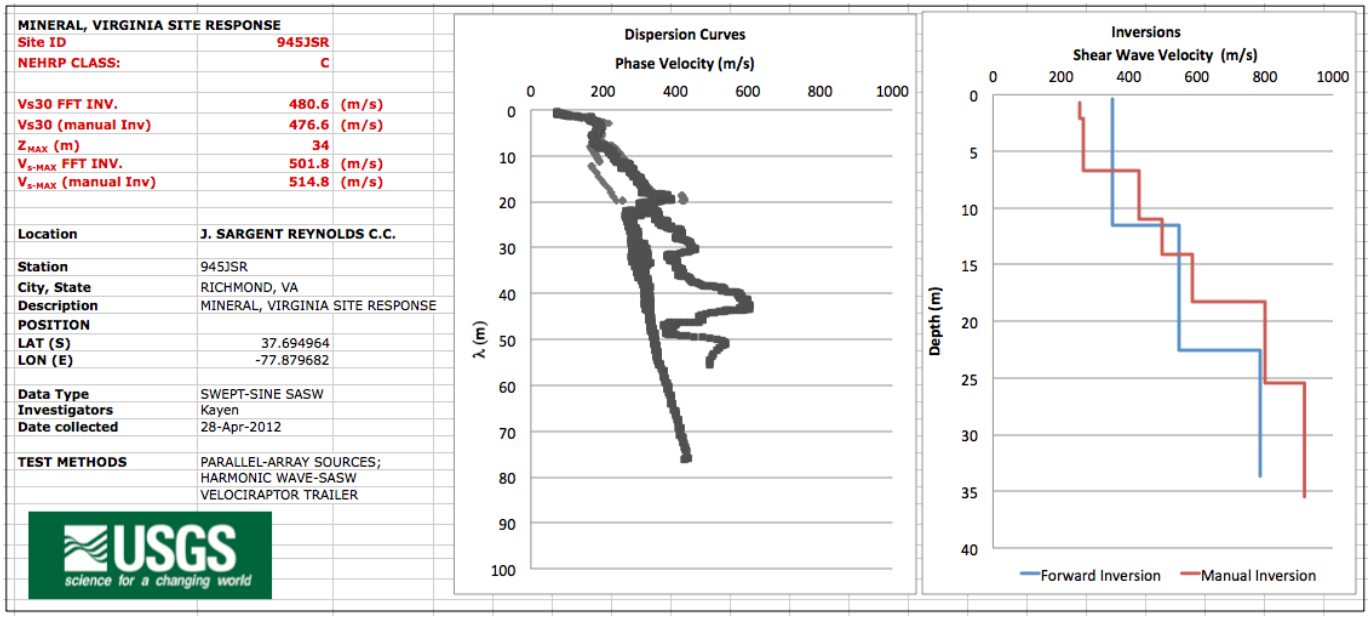

Figure 1–19. Site ID, location, and average shear wave velocity (left) for surface wave test site 945JSR; average dispersion curve in dark gray and individual empirical dispersion curves in lighter gray (center plot); shear wave velocity profiles computed by two inversion methods (right plot).

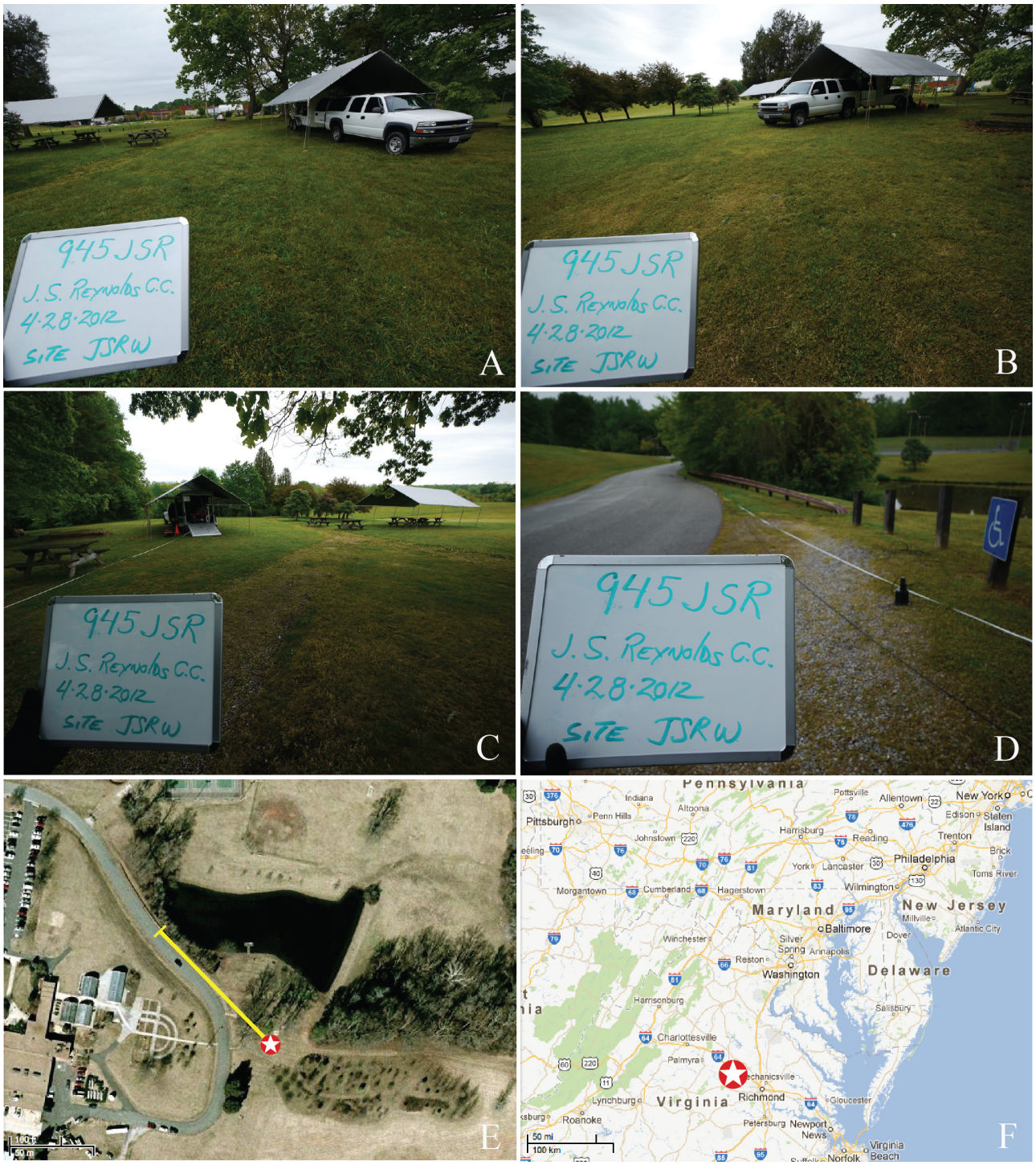

Figure 1–20. Surface wave test site 945JSR located at J. Sargeant Reynolds Community College, Goochland, Virginia (lat 37.6952, long −77.8798). A, Photo looking northwest towards the shaker trailer parked beneath the covering. B, View southward toward the shaker trailer. C, View southeast to the shaker trailer. D, View to the northwest along the seismometer array. E, Satellite view of the local site, yellow bar is seismometer array. F, Site location near Goochland, Va.

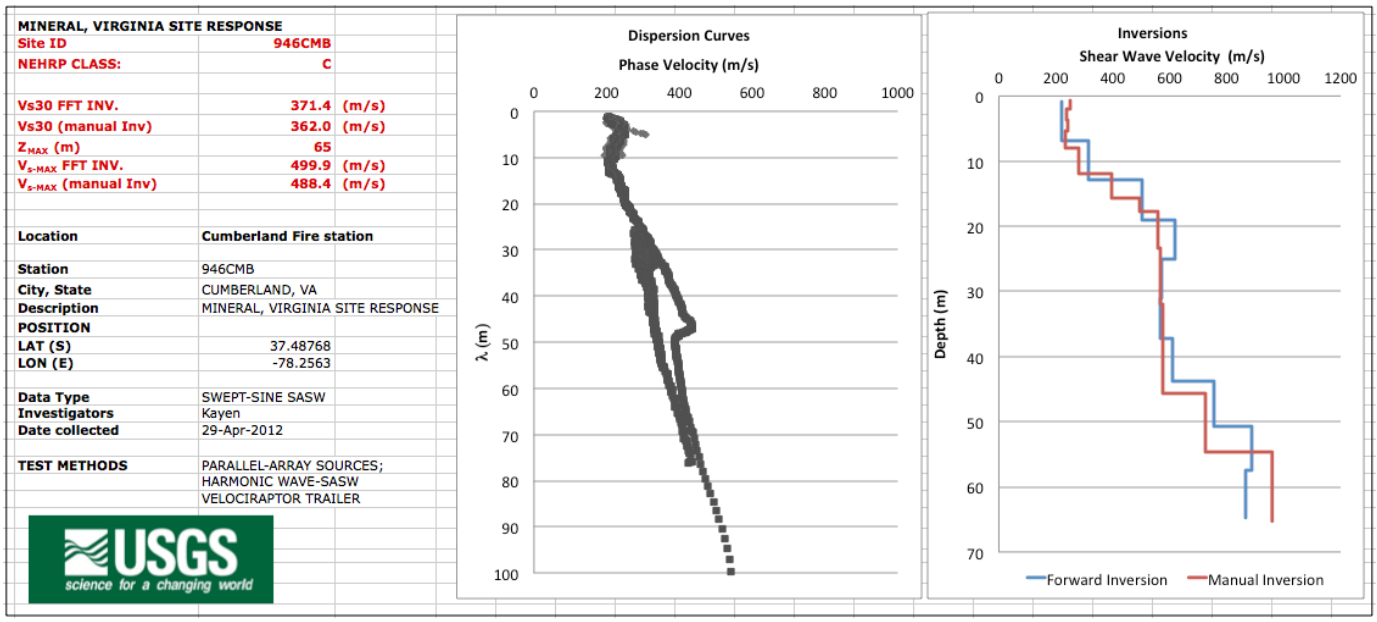

Figure 1–21. Site ID, location, and average shear wave velocity (left) for surface wave test site 946CMB; average dispersion curve in dark gray and individual empirical dispersion curves in lighter gray (center plot); shear wave velocity profiles computed by two inversion methods (right plot).

Figure 1–22. Surface wave test site 946CMB located at the volunteer rescue squad fire station, Cumberland, Virginia (lat 37.4881, long −78.2563). A, View looking southeast towards the shaker trailer and trend of the seismometer array. B, View northwest to the shaker trailer. C, View from the shaker trailer southwest to the fire station. D, Another view to the southeast along the direction of the seismometer array. E, Satellite view of the local site, yellow bar is seismometer array. F, Site location in Cumberland, Va.

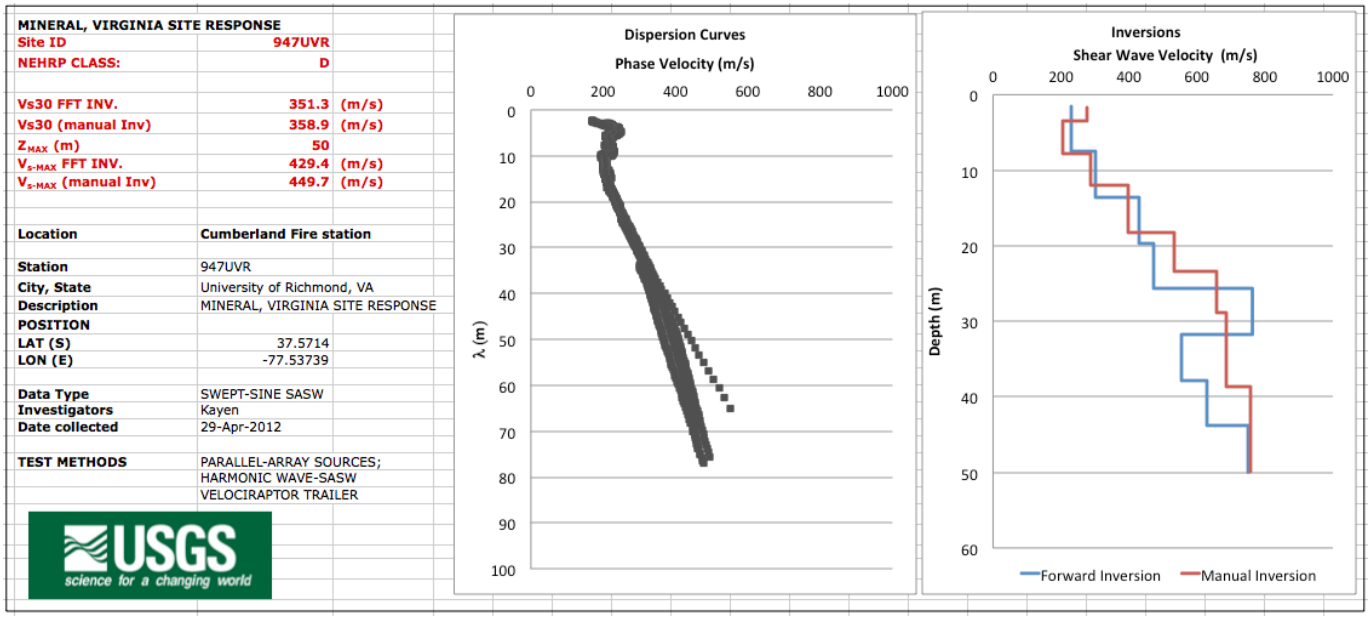

Figure 1–23. Site ID, location, and average shear wave velocity (left) for surface wave test site 947UVR; average dispersion curve in dark gray and individual empirical dispersion curves in lighter gray (center plot); shear wave velocity profiles computed by two inversion methods (right plot).

Figure 1–24. Surface wave test site 947UVR located at the east margin of the intramural fields, University of Richmond, Richmond, Virginia (lat 37.5709, long −77.5374). A, View to the north to the shaker trailer. B, Another view northward to the shaker trailer. C, View west to the shaker trailer. D, View to the south along the seismometer array toward the shaker trailer. E, satellite view of the local site, yellow bar is seismometer array. F, Site location in Richmond, Va.

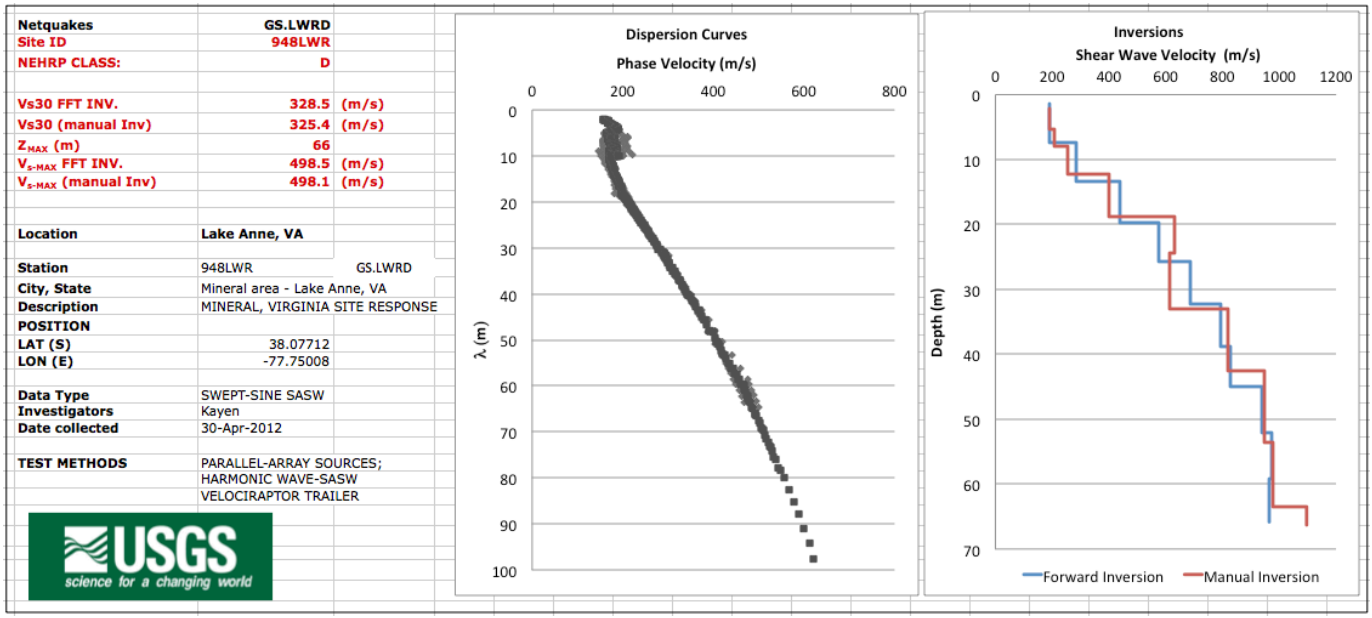

Figure 1–25. Site ID, location, and average shear wave velocity (left) for surface wave test site 948LWR; average dispersion curve in dark gray and individual empirical dispersion curves in lighter gray (center plot); shear wave velocity profiles computed by two inversion methods (right plot).

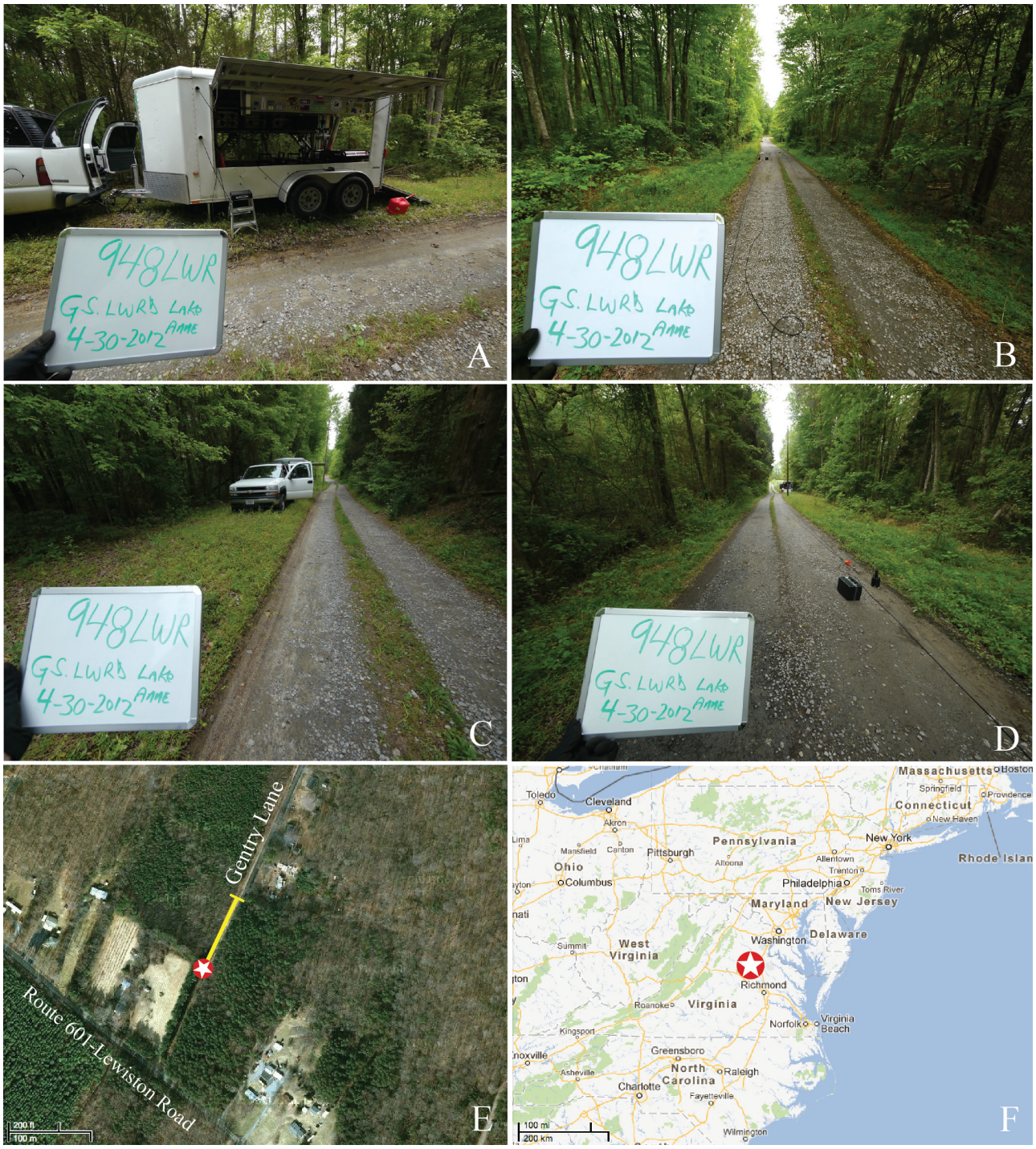

Figure 1–26. Surface wave test site 948LWR located on Gentry Lane about 16 kilometers northeast of Mineral, Virginia, and 66 kilometers northwest of Richmond, Virginia (lat 38.0796, long −77.7515). A, View looking northwest to the shaker trailer on Gentry Lane. B, View north-northeast from the shaker trailer to the seismometer array. C, Another view to the north-northeast to the shaker trailer. D, View to the south-southwest along seismometer array to the shaker trailer. E, Satellite view of the local site, yellow bar is seismometer array. F, Site location northwest of Richmond, Va.

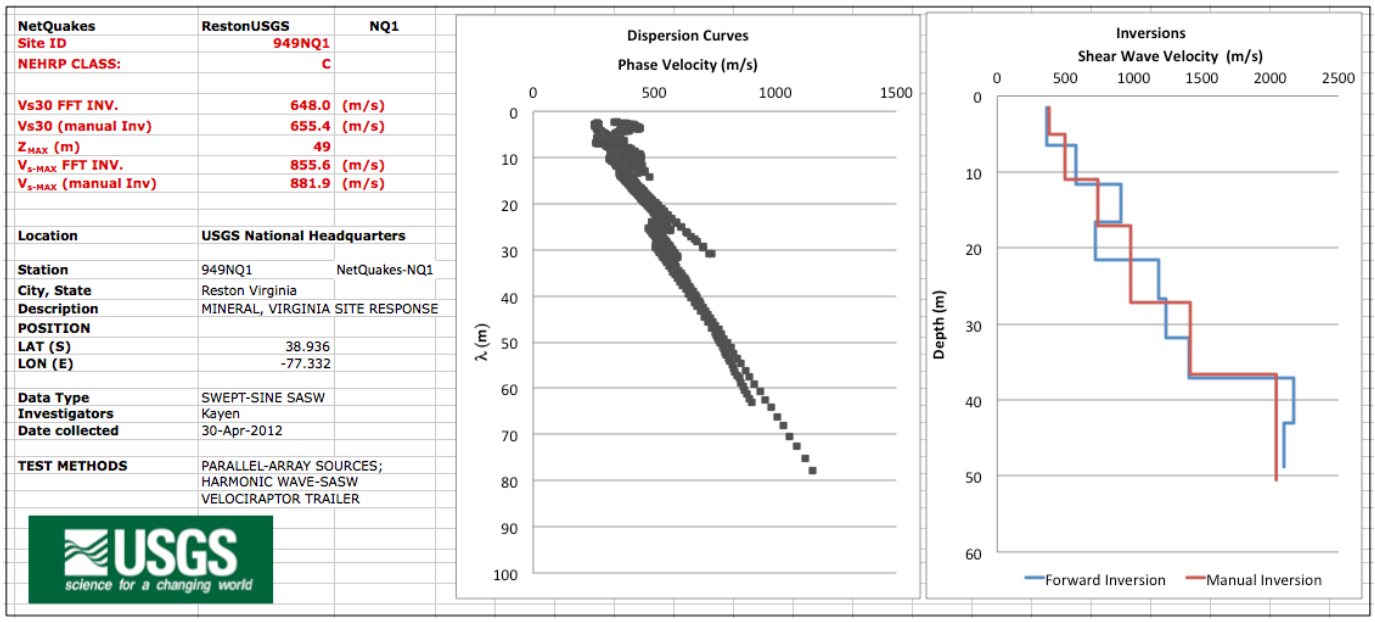

Figure 1–27. Site ID, location, and average shear wave velocity (left) for surface wave test site 949NQ1; average dispersion curve in dark gray and individual empirical dispersion curves in lighter gray (center plot); shear wave velocity profiles computed by two inversion methods (right plot).

Figure 1–28. Surface wave test site 949NQ1 located at the U.S. Geological Survey National Center in Reston, Virginia (lat 38.9477, long −77.3673). A, View looking southeast from the shaker trailer to the seismometer array. B, View northwest to the shaker trailer. C, View to the north to the shaker trailer and near-end of the seismometer array. D, Closer view of the shaker trailer looking north. E, Satellite view of the local site, yellow bar is seismometer array. F, Site location in Reston, Va.

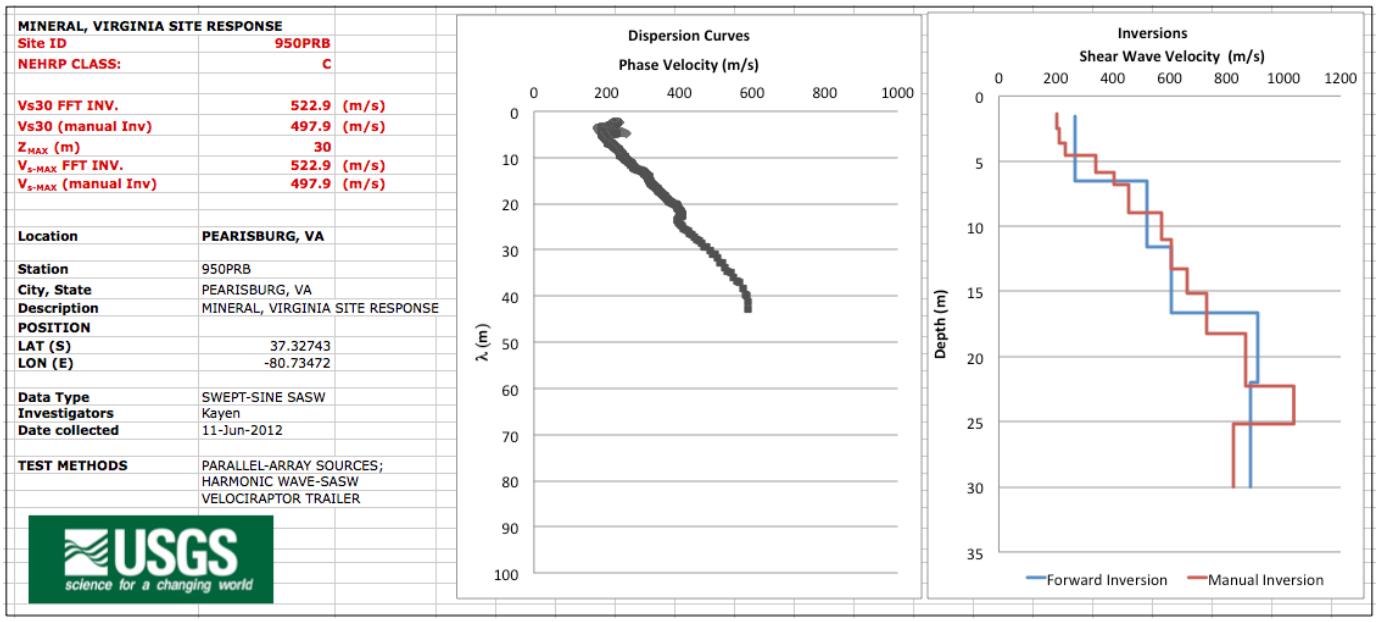

Figure 1–29. Site ID, location, and average shear wave velocity (left) for surface wave test site 950PRB; average dispersion curve in dark gray and individual empirical dispersion curves in lighter gray (center plot); shear wave velocity profiles computed by two inversion methods (right plot).

Figure 1–30. Surface wave test site 950PRB located next to city/county buildings in Pearisburg, Virginia (lat 37.3275, long −80.7345). A, View looking southwest to the shaker trailer, Giles County courthouse in the background. B, View west-southwest down the seismometer array from the shaker trailer. C, View east-northeast to the shaker trailer from near the far end of the array. D, Closer view of the shaker trailer looking east-northeast. E, Satellite view of the local site, yellow bar is seismometer array. F, Site location in Pearisburg, Va.

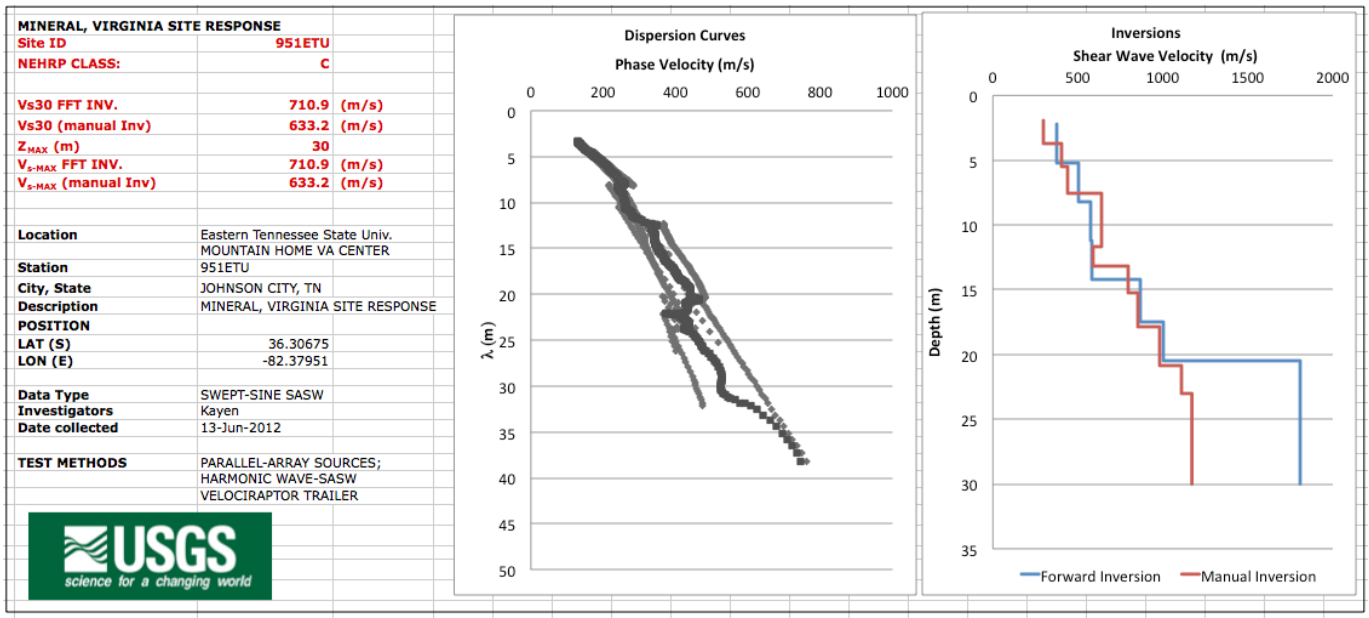

Figure 1–31. Site ID, location, and average shear wave velocity (left) for surface wave test site 951ETU; average dispersion curve in dark gray and individual empirical dispersion curves in lighter gray (center plot); shear wave velocity profiles computed by two inversion methods (right plot).

Figure 1–32. Surface wave test site 951ETU located adjacent to Building 52, James H. Quillen College of Medicine, East Tennessee State University, Johnson City, Tennessee (lat 36.307, long −82.3795). A, View eastward to the shaker trailer. B, View westward to the seismometer array. C, Another view eastward to the shaker trailer. D, Limestone bedrock outcrop about 500 meters east-northeast of the shaker trailer location. E, Satellite view of the local site, yellow bar is seismometer array. F, Site location in Johnson City, Tenn.

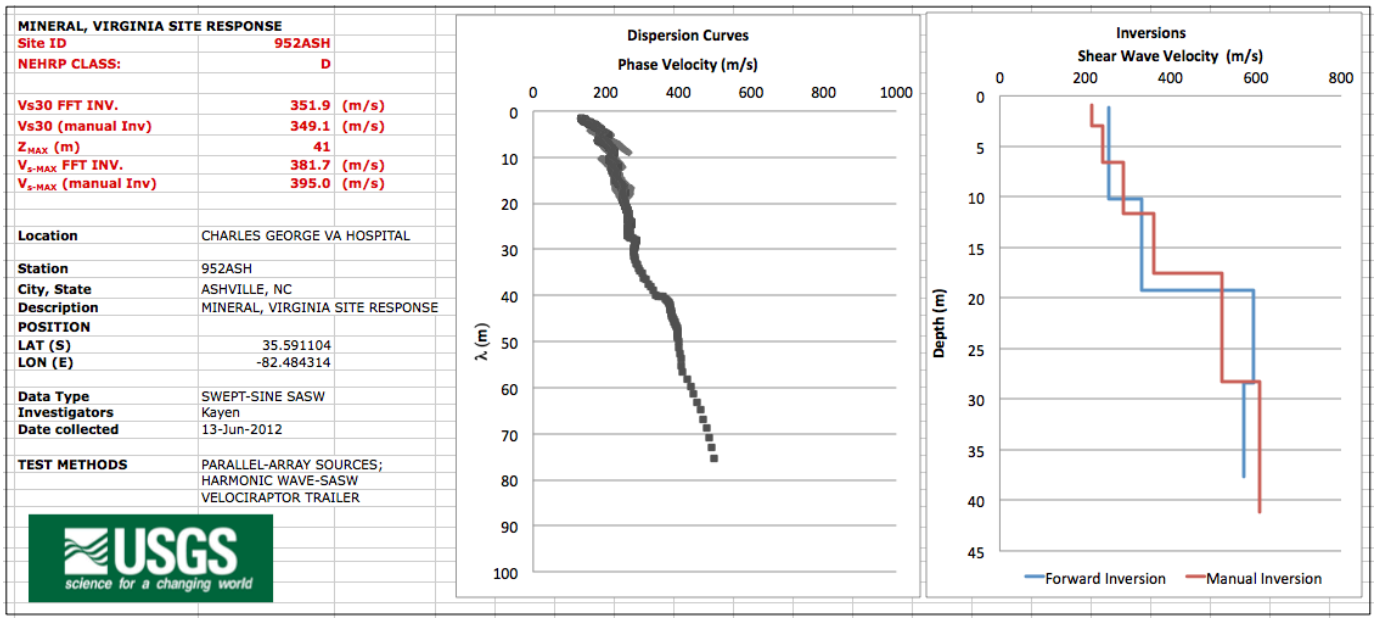

Figure 1–33. Site ID, location, and average shear wave velocity (left) for surface wave test site 952ASH; average dispersion curve in dark gray and individual empirical dispersion curves in lighter gray (center plot); shear wave velocity profiles computed by two inversion methods (right plot).

Figure 1–34. Surface wave test site 952ASH located at the Charles George VA Medical Center, Asheville, North Carolina (lat 35.5912, long −82.4844). A, View looking northwest toward the shaker trailer. B, View east to the seismometer array. C, View west to the shaker trailer from the seismometer array. D, View to the southeast of the shaker trailer. E, Satellite view of the local site, yellow bar is seismometer array. F, Site location in Asheville, N.C.

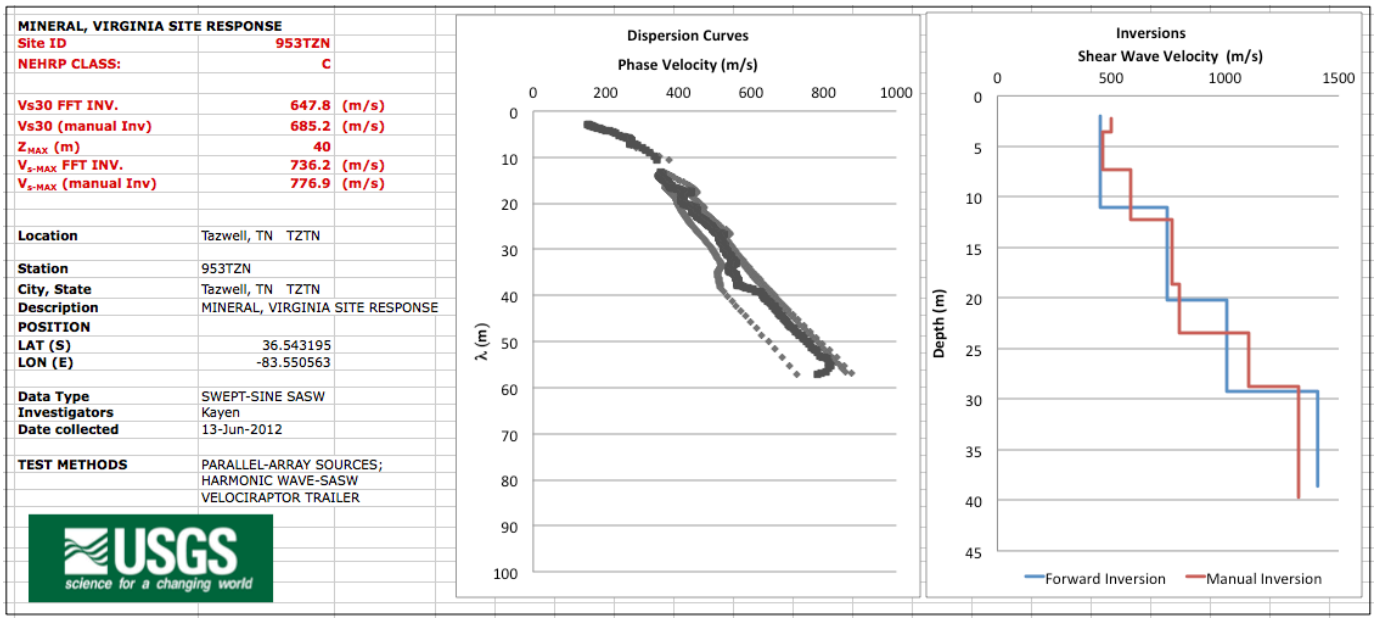

Figure 1–35. Site ID, location, and average shear wave velocity (left) for surface wave test site 953TZN; average dispersion curve in dark gray and individual empirical dispersion curves in lighter gray (center plot); shear wave velocity profiles computed by two inversion methods (right plot).

Figure 1–36. Surface wave test site 953TZN located on Parks Lane about 10 kilometers north-northeast of Tazewell, Tennessee (lat 36.5433, long −83.5504). A, View looking northeast towards the shaker trailer. B, View looking south from the shaker trailer. C, View southwest from shaker trailer to the seismometer array. D, View eastward to the shaker trailer. E, Satellite view of the local site, yellow bar is seismometer array. F, Site location near Tazewell, Tenn.

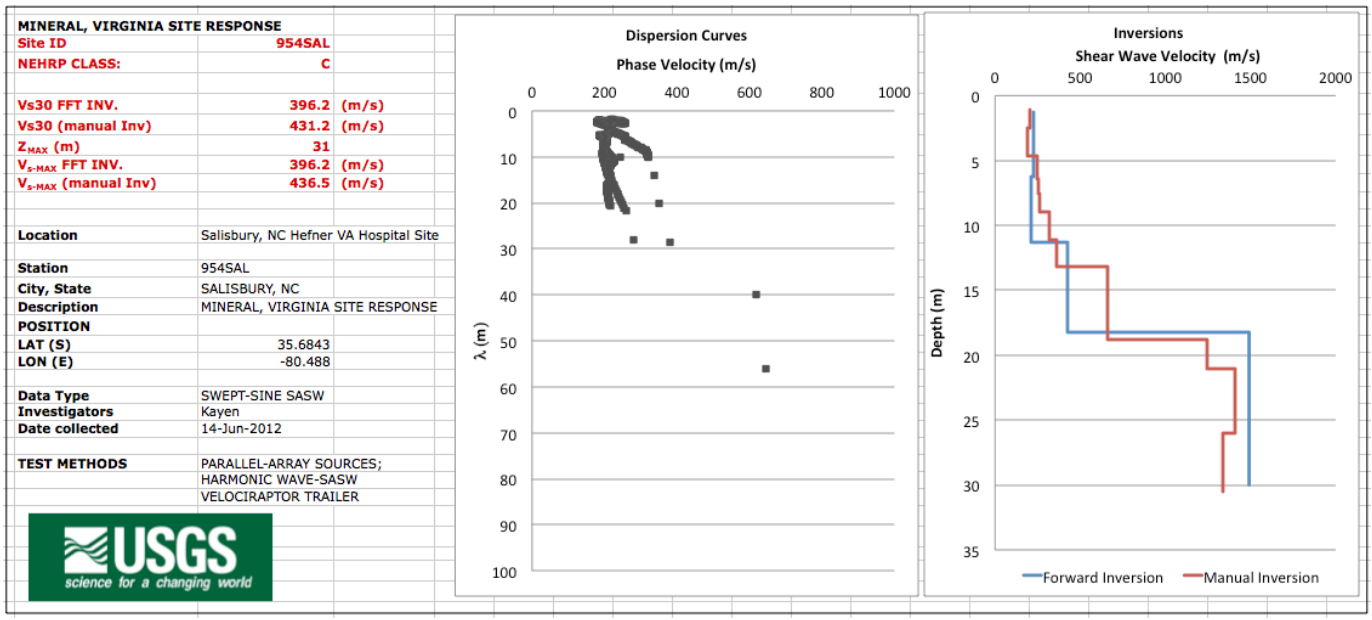

Figure 1–37. Site ID, location, and average shear wave velocity (left) for surface wave test site 954SAL; average dispersion curve in dark gray and individual empirical dispersion curves in lighter gray (center plot); shear wave velocity profiles computed by two inversion methods (right plot).

Figure 1–38. Surface wave test site 954SAL located at the Hefner VA Medical Center, Salisbury, North Carolina (lat 35.6851, long −80.4888). A, View westward to the shaker trailer. B, View to the north along the seismometer array. C, View to the southeast across the seismometer array, shaker trailer on the right. D, View to the northwest from the shaker trailer. E, Satellite view of the local site, yellow bar is seismometer array. F, Site location in Salisbury, N.C.

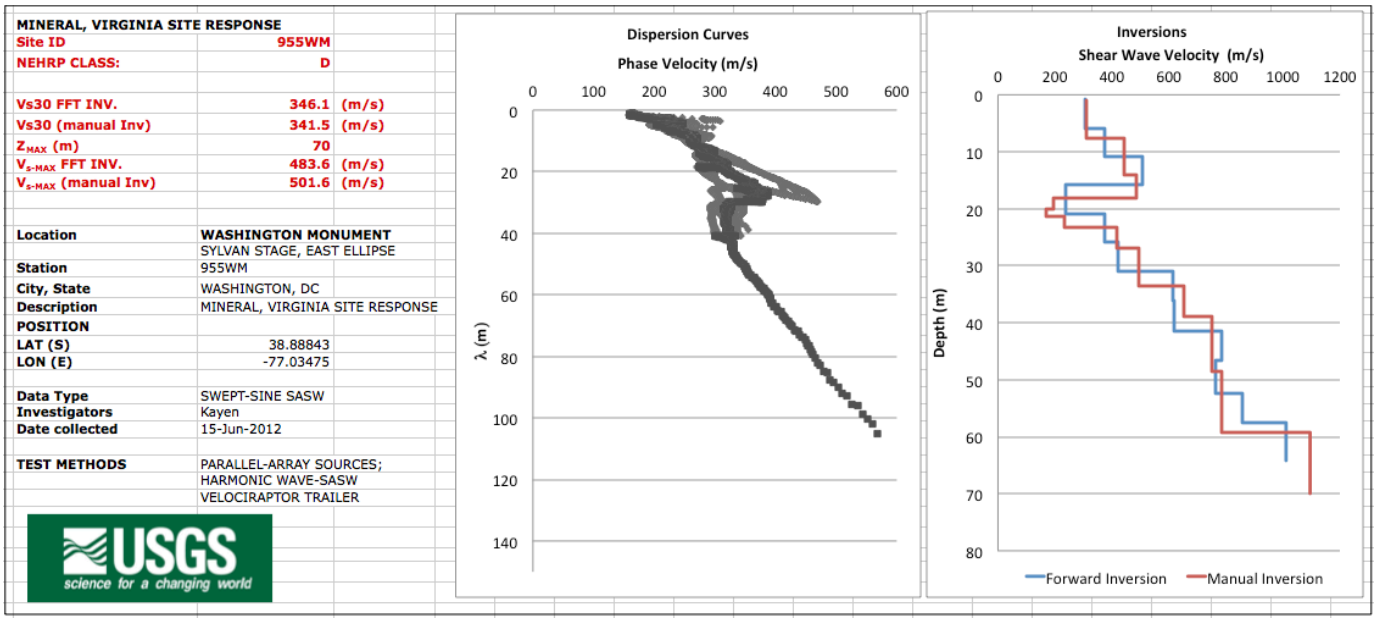

Figure 1–39. Site ID, location, and average shear wave velocity (left) for surface wave test site 955WM; average dispersion curve in dark gray and individual empirical dispersion curves in lighter gray (center plot); shear wave velocity profiles computed by two inversion methods (right plot).

Figure 1–40. Surface wave test site 955WM located at the Washington Monument, Washington, D.C. (lat 38.8885, long −77.0346). A, View looking northwest from the Sylvan Theater stage towards the Washington Monument and shaker trailer. B, View southwest to the shaker trailer. C, View southward to the shaker trailer, Sylvan Theater in the background. D, View looking northwest to the Monument and the seismometer array crossing the path. E, Satellite view of the local site, yellow bar is seismometer array. F, Site location in Washington, D.C.

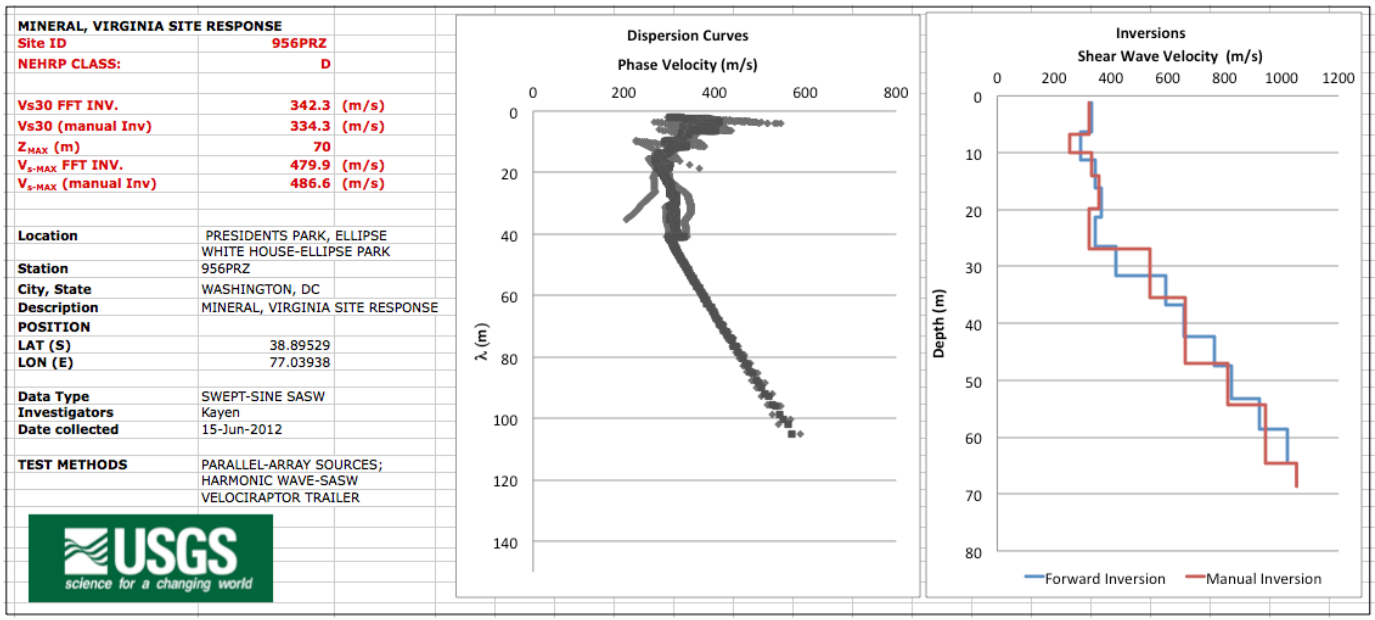

Figure 1–41. Site ID, location, and average shear wave velocity (left) for surface wave test site 956PRZ; average dispersion curve in dark gray and individual empirical dispersion curves in lighter gray (center plot); shear wave velocity profiles computed by two inversion methods (right plot).

Figure 1–42. Surface wave test site 956PRZ located at President's Park at the intersection of 17th Street NW and E Street NW near the northwest margin of The Ellipse (lat 38.8952, long −77.0394). A, View north towards to the shaker trailer on 17th Street. B, View south to the shaker trailer on 17th Street. C, View of the shaker trailer looking west. D, View northwest to the shaker trailer. E, Satellite view of the local site, yellow bar is seismometer array. F, Site location in Washington, D.C.

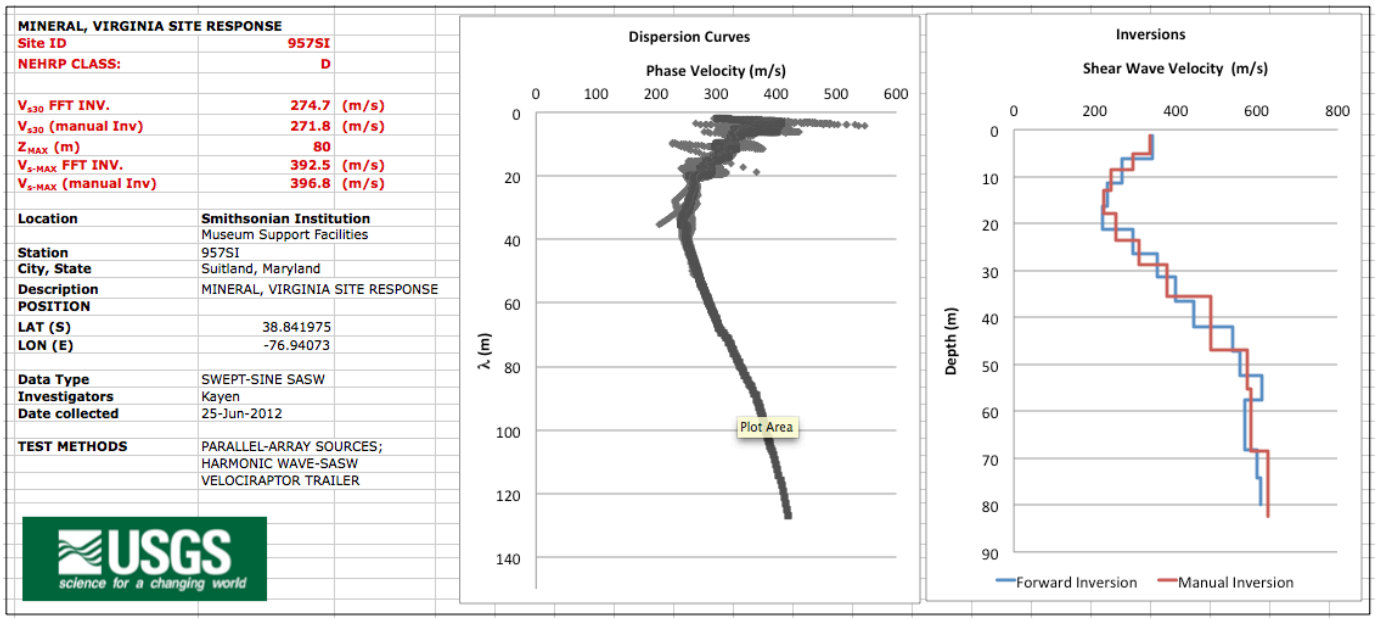

Figure 1–43. Site ID, location, and average shear wave velocity (left) for surface wave test site 957SI; average dispersion curve in dark gray and individual empirical dispersion curves in lighter gray (center plot); shear wave velocity profiles computed by two inversion methods (right plot).

Figure 1–44. Surface wave test site 957SI located at the Smithsonian Archive Warehouse, Suitland, Maryland (lat 38.84195, long −76.9408). A, View looking east-southeast along the seismometer array towards the shaker trailer. B, View northwest from the shaker trailer toward the seismometer array. C, View to the southeast of the shaker trailer. D, Students and researchers from Lehigh University, Virginia Tech, and the U.S. Geological Survey gathered at the test site. E, Satellite view of the local site, yellow bar is seismometer array. F, Site location in Suitland, Md.

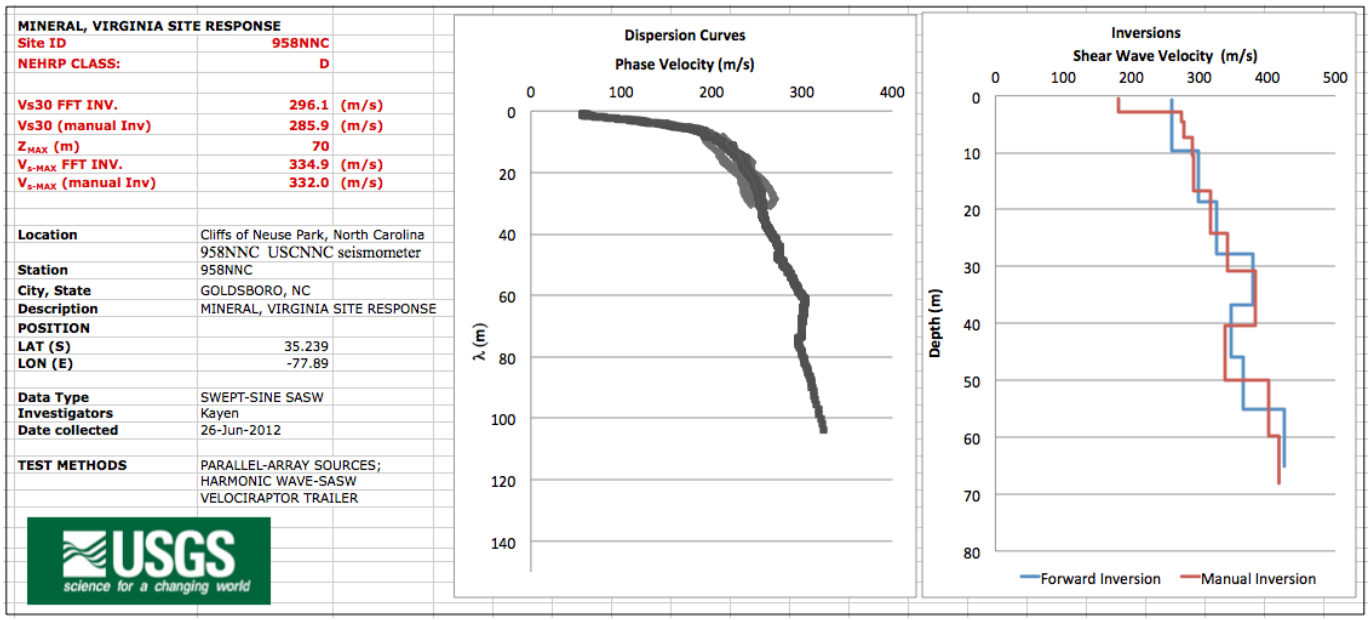

Figure 1–45. Site ID, location, and average shear wave velocity (left) for surface wave test site 958NNC; average dispersion curve in dark gray and individual empirical dispersion curves in lighter gray (center plot); shear wave velocity profiles computed by two inversion methods (right plot).

Figure 1–46. Surface wave test site 958NNC located at the Cliffs of the Neuse State Park, Seven Springs, North Carolina, about 18 kilometers southeast of Goldsboro (lat 35.2398, long −77.8906). A, View looking northeast from the shaker trailer along the seismometer array. B, View looking southwest toward the shaker trailer. C, View southward to the shaker trailer and tow vehicle. D, Another view southward to the shaker trailer. E, Satellite view of the local site, yellow bar is seismometer array. F, Site location near Seven Springs, N.C.

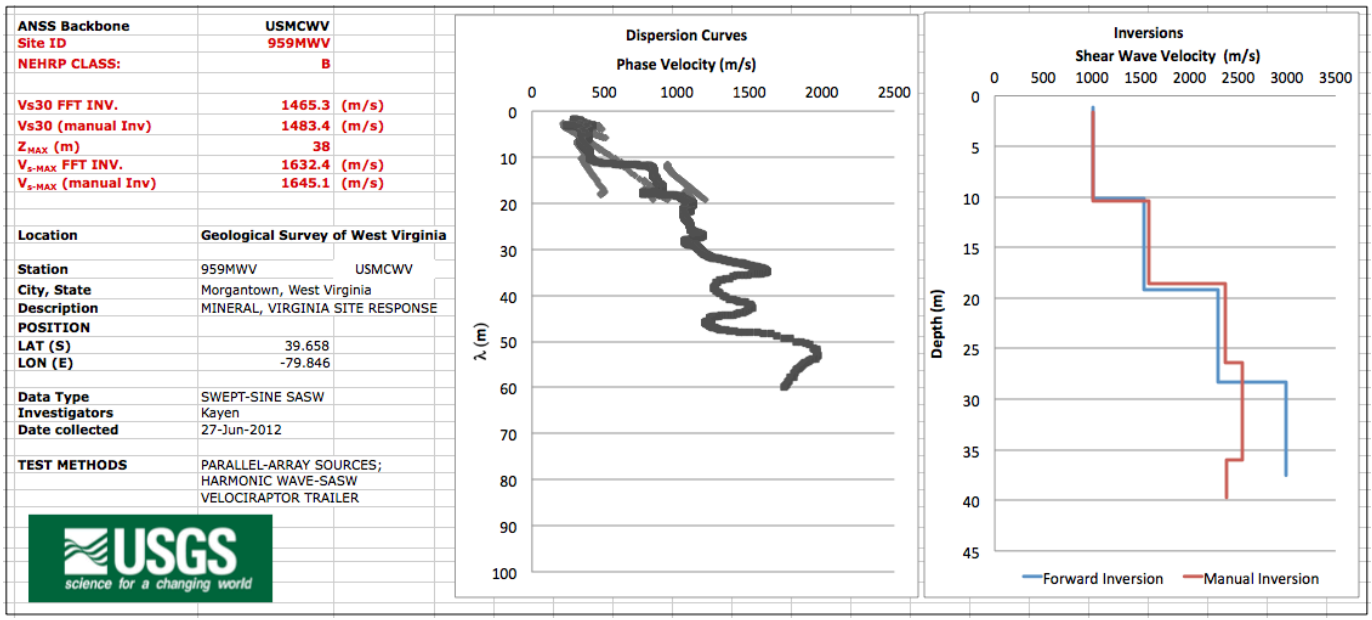

Figure 1–47. Site ID, location, and average shear wave velocity (left) for surface wave test site 959MWV; average dispersion curve in dark gray and individual empirical dispersion curves in lighter gray (center plot); shear wave velocity profiles computed by two inversion methods (right plot).

Figure 1–48. Surface wave test site 959MWV located at the West Virginia Geological & Economic Survey, Morgantown, West Virginia (lat 39.6594, long −79.8499). A, View looking southeast towards the seismometer array in the upper parking lot. B, Another view southeast toward the shaker trailer. C, View southeast toward the shaker trailer at the entrance gate. D, View to the northwest of the shaker trailer. E, Satellite view of the local site, yellow bar is seismometer array. F, Site location near Morgantown, W. Va.